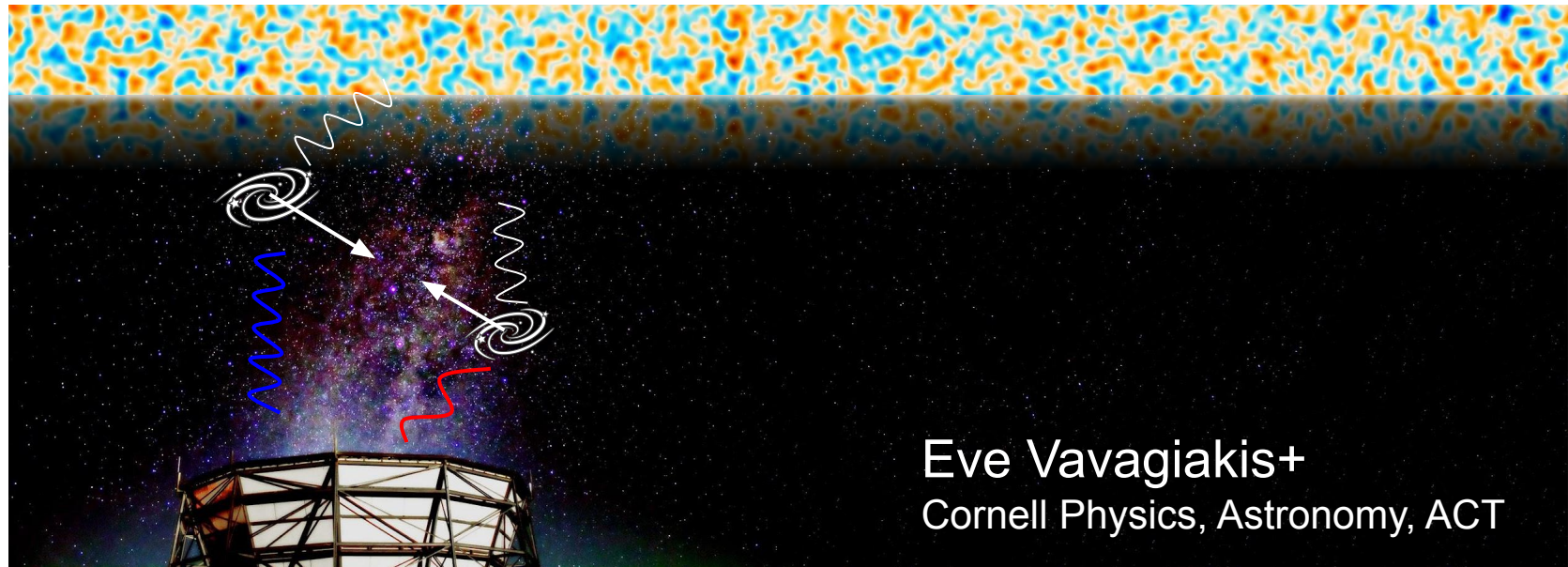
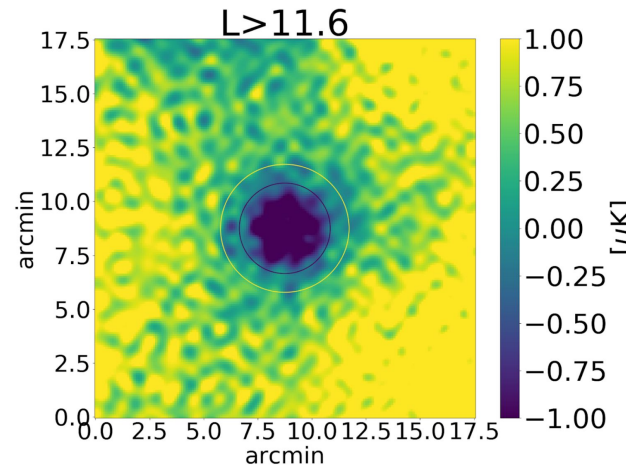
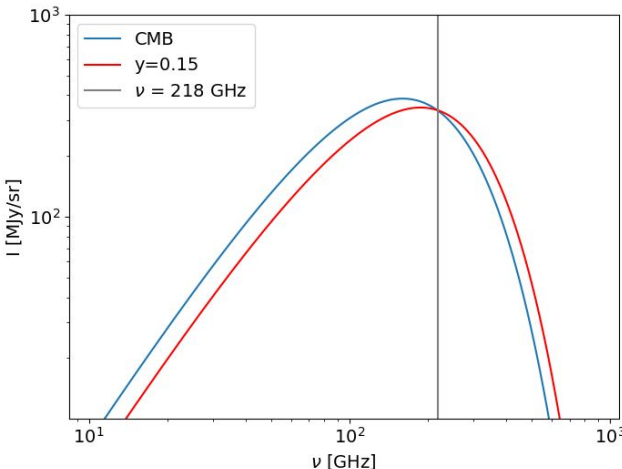


# Current measurements and future prospects: Pairwise kSZ



# The Sunyaev Zel'dovich Effects

- Thermal SZ effect:
  - Sensitive to integrated line-of-sight pressure profile
  - Can break optical depth degeneracy
- Kinematic SZ effect:
  - Doppler shift in CMB temperature due to bulk motion
  - Break optical depth degeneracy for cosmology



$$\frac{\Delta T(\nu)}{T_{\text{CMB}}} = f(\nu) \frac{\sigma_{\text{T}}}{m_{\text{e}}c^2} \int_{\text{LOS}} n_{\text{e}} k T_{\text{e}} \text{d}l$$

$$\frac{\delta T_{\text{kSZ}}(\hat{n})}{T_{\text{CMB}}} = -\tau_{\text{gal}} \left( \frac{v_{e,r}}{c} \right)$$

(Cluster astrophysics)x(Cosmology)

$$\tau = \sigma_{\text{T}} \int_{\text{LOS}} n_{\text{e}} \text{d}l$$

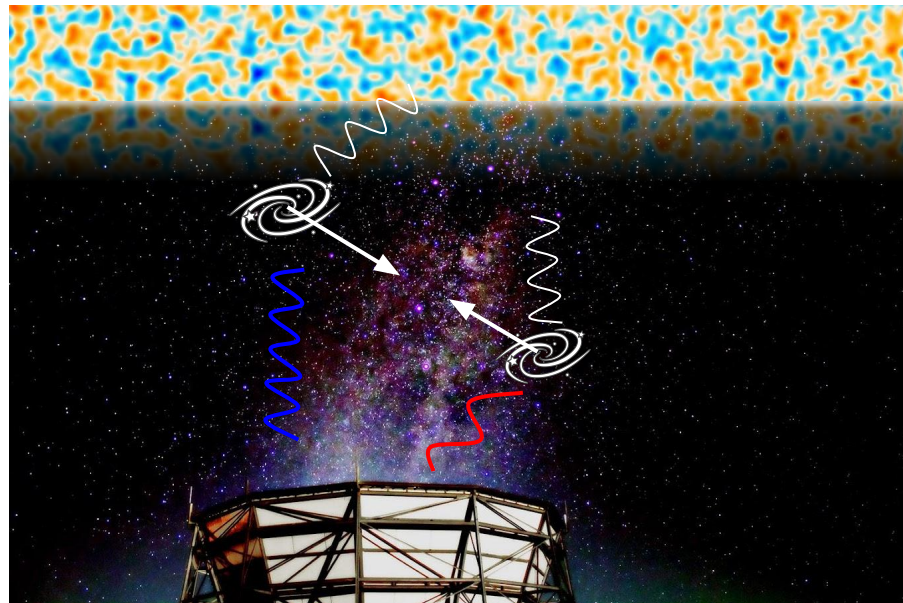
A backlight on baryons:

Both SZ effects

∞ halo optical depth ( $\tau$ )

# Pairwise kSZ Estimator

- Differential statistic probing the mean relative motion of galaxies
  - Use temperature signal pairs



$$\frac{\delta T_{\text{kSZ}}(\hat{\mathbf{n}})}{T_{\text{CMB}}} = -\tau_{\text{gal}} \left( \frac{v_{e,r}}{c} \right)$$

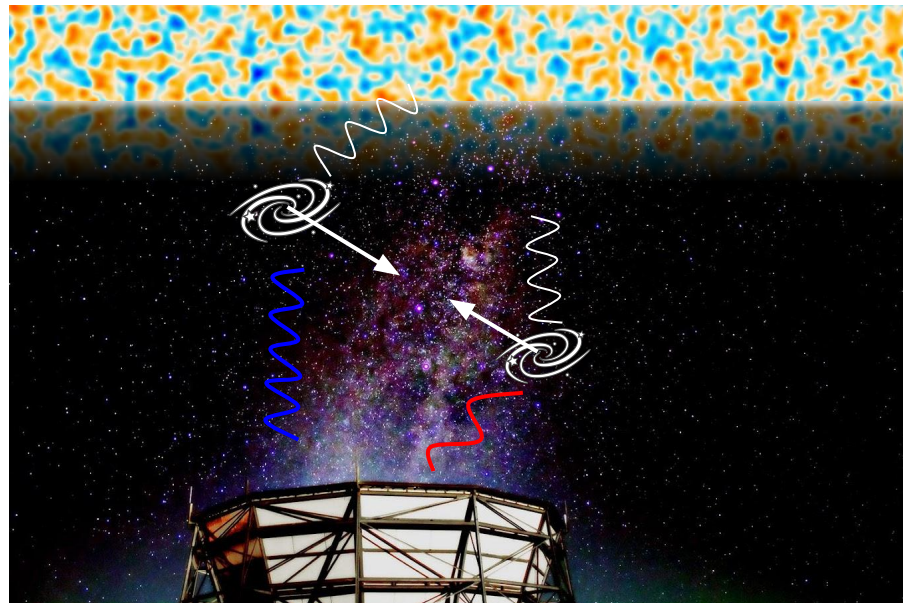
$$\delta T_{\text{kSZ}}(\hat{\mathbf{n}}) \propto -\mathbf{p}_i \cdot \mathbf{r}_i$$

$$\hat{p}(r) = -\frac{\sum_i (\delta T_i - \bar{\delta T}) c_{ij}}{\sum_{i < j} c_{ij}^2}$$

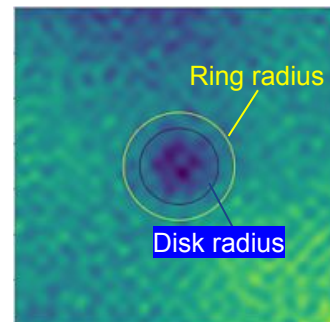
Geometrical factor  
depending on redshift

# Pairwise kSZ Estimator

- Positions and redshifts from optical catalog
- Sum over temperature signal differences in comoving separation bins



$$\frac{\delta T_{\text{kSZ}}(\hat{\mathbf{n}})}{T_{\text{CMB}}} = -\tau_{\text{gal}} \left( \frac{v_{e,r}}{c} \right)$$

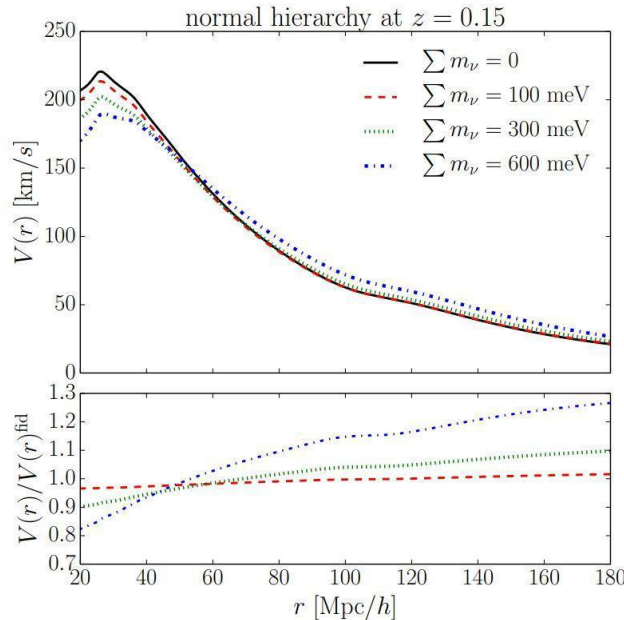


$$\delta T_{\text{kSZ}} = T_{\text{disk}} - T_{\text{ring}}$$

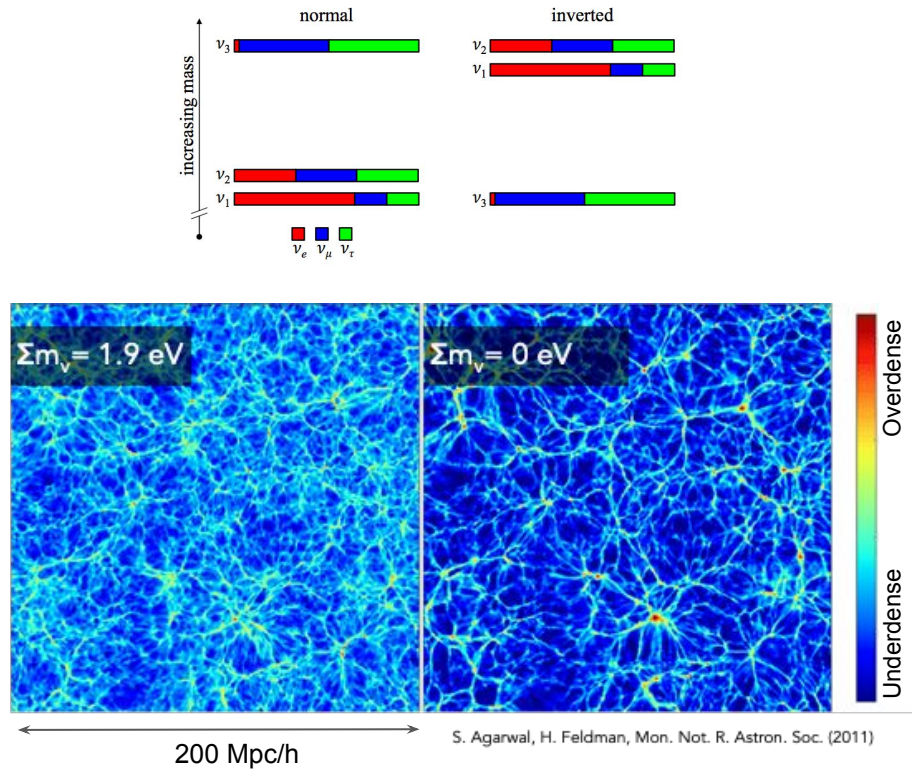
$$\hat{p}(r) = -\frac{\sum (\delta T_i - \delta T_j) c_{ij}}{\sum_{i < j} c_{ij}^2}$$

# Pairwise kSZ Prospects

- Constrain neutrino mass sum,  $\sigma_8$ ,  $f$ , dark energy, models of modified gravity, baryon content



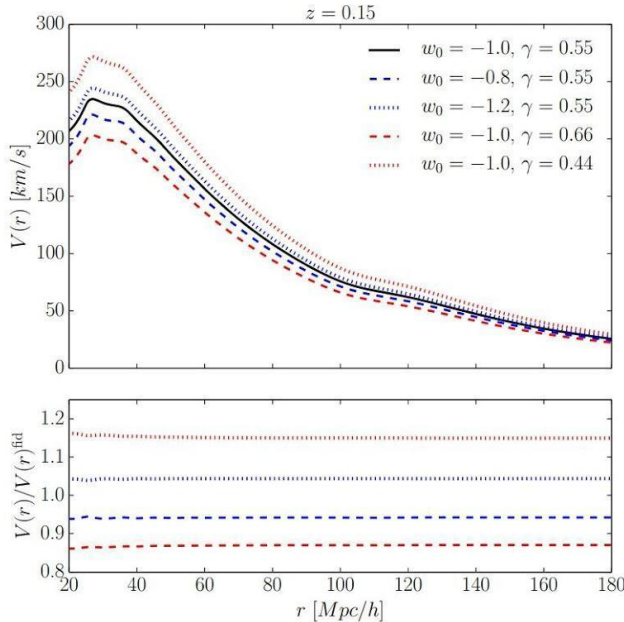
E. M. Mueller, F. de Bernardis, R. Bean, M. D. Niemack (2014), 1412.0592



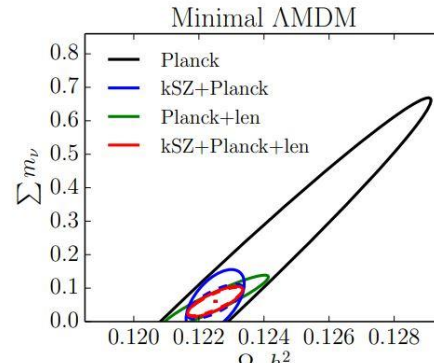
S. Agarwal, H. Feldman, Mon. Not. R. Astron. Soc. (2011)

# Pairwise kSZ Prospects

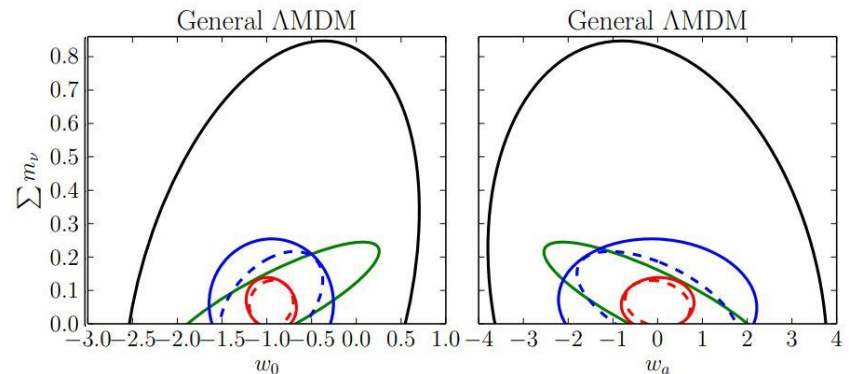
- Constrain neutrino mass sum,  $\sigma_8$ ,  $f$ , dark energy, models of modified gravity, baryon content



E. M. Mueller, F. de Bernardis, R. Bean, M. D. Niemack (2014), 1408.6248



E. M. Mueller, F. de Bernardis, R. Bean, M. D. Niemack (2014), 1412.0592



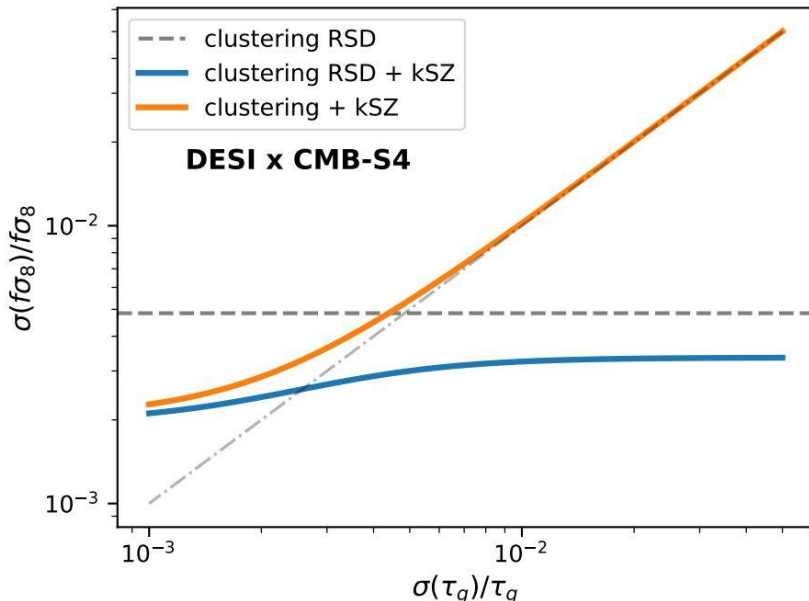
# Pairwise kSZ Prospects

growth rate of density perturbations

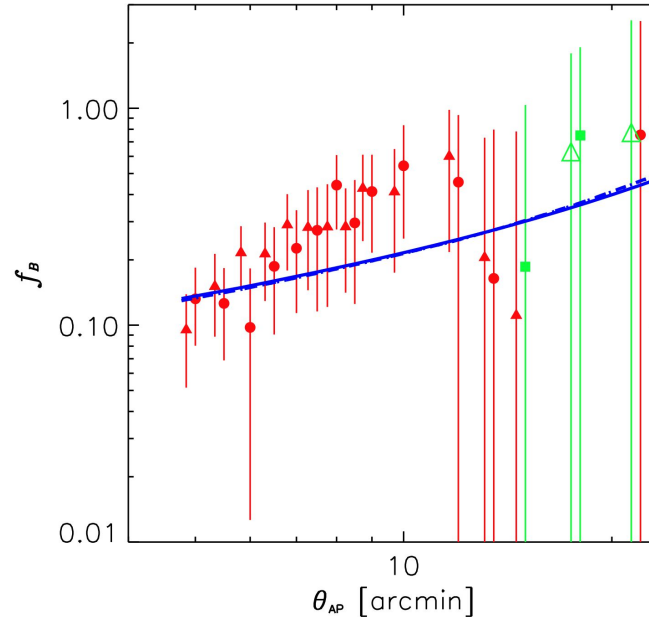
matter fluctuations 8 Mpc/h

$$\propto \bar{\tau}_e \times f \sigma_8^2$$

- Constrain neutrino mass sum,  $\sigma_8$ ,  $f$ , dark energy, models of modified gravity, baryon content



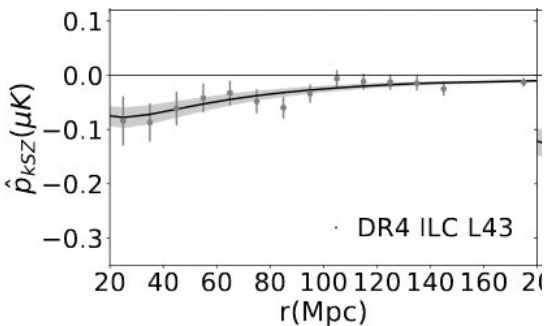
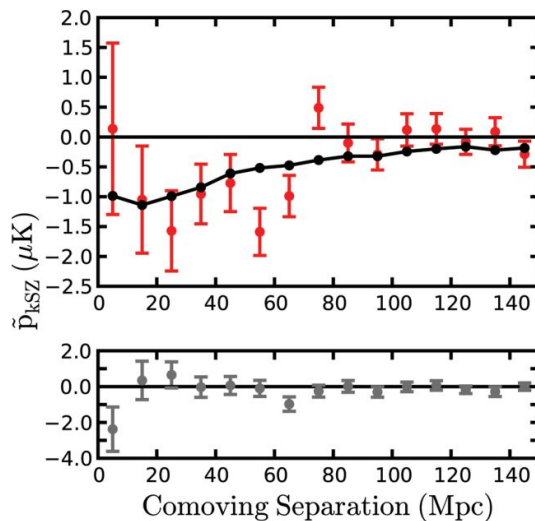
CMB-S4 Science Case, arXiv:1907.04473



Hernández-Monteagudo et al. 2015 Phys. Rev. Lett. 115, 191301

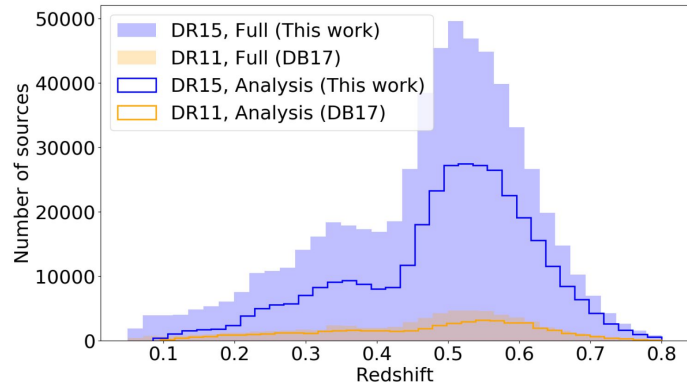
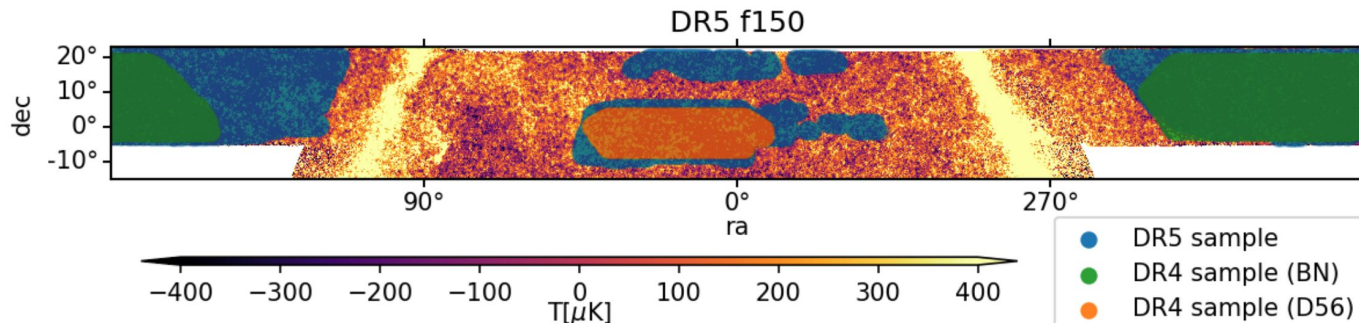
# Pairwise kSZ Measurements

- N. Hand et al. 2012, ACT & SDSS (arXiv:1203.4219)
  - First kSZ detection,  $p=0.002$
- F de Bernardis et al. 2017, ACT & SDSS (arXiv:1607.02139)
  - $4.1\sigma$  and tSZ/kSZ comparison
- Planck 2015 (arXiv:1504.03339)
  - $1.8\text{-}2.5\sigma$
- SPT & DES 2016 (arXiv:1603.03904)
  - $4.2\sigma$
- Calafut et al. 2021, ACT+Planck & SDSS (arXiv:2101.08374)
  - $5.4\sigma$



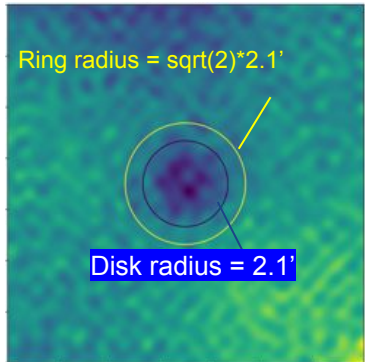
# Pairwise kSZ with ACT, *Planck*, and SDSS

- ACT+*Planck* coadded maps at 150, 98 GHz (Naess et al. 2020, arXiv:2007.07290)
- Component separated Compton-y, CMB+kSZ maps (Madhavacheril et al. 2019, arXiv:1911.05717)
- Selected BOSS-SDSS DR15 galaxies, three disjoint luminosity bins for joint SZ analysis



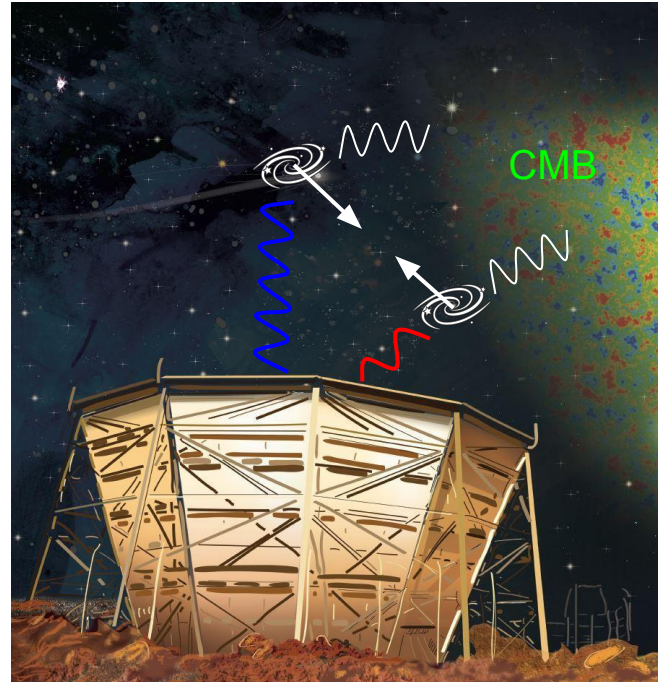
# Pairwise kSZ with ACT, *Planck*, and SDSS

- Aperture photometry on source-centered submaps:  
2.1' radius aperture
- Pairwise estimator for kSZ measurement  
w/bootstrap uncertainties



$$\delta T_i = T_{\text{disk}} - T_{\text{ring}}$$

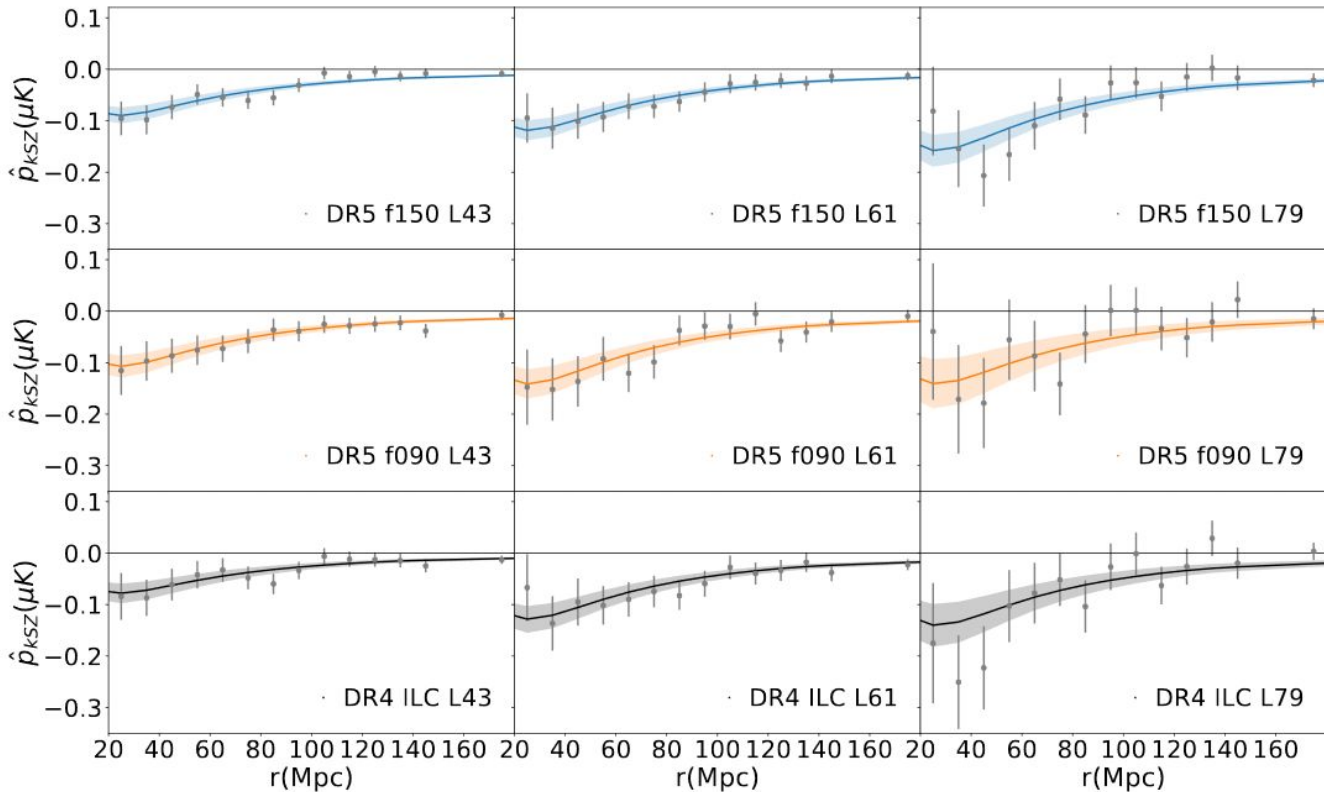
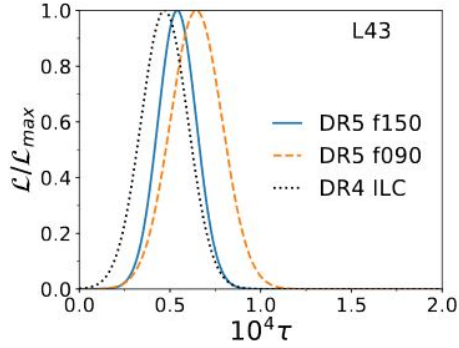
$$\hat{p}(r) = - \frac{\sum (\delta T_i - \delta T_j) c_{ij}}{\sum_{i < j} c_{ij}^2}$$



# Pairwise kSZ ACT, Planck, SDSS results

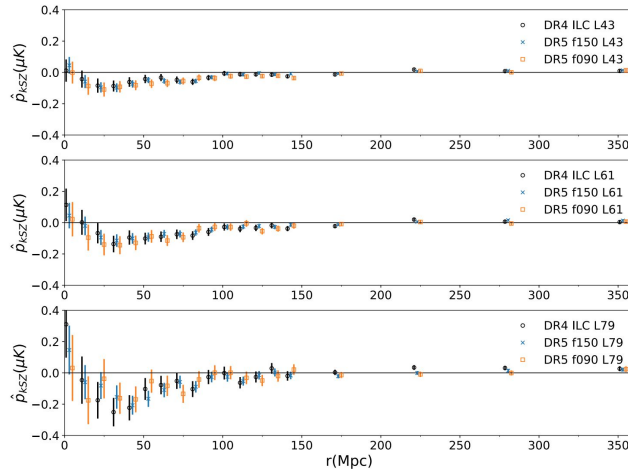
$$\hat{p}_{\text{th}}(r, z) = -\frac{T_{CMB}}{c} \bar{\tau} V(r, z)$$

- 5.4 $\sigma$  detection
- Fits to model yield estimate of optical depth, trace baryon content
- Consistent across maps

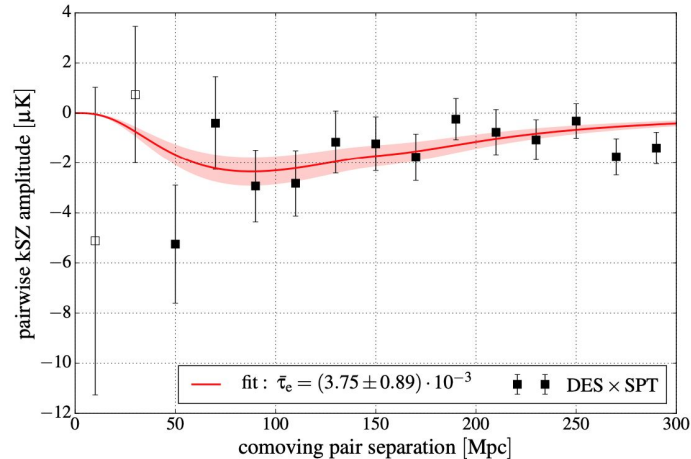


# ACT+*Planck*, SDSS (2021) versus SPT, DES (2016)

- ~3,700 sq. deg. of SDSS DR15 data overlapping with ACT+*Planck* DR5
- 343,647 sources with spectroscopic redshifts  $0.08 < z < 0.8$
- Aperture photometry filter
- $\tau \sim (0.69 \pm 0.11) \times 10^{-4}$ ,  $5.4\sigma$
- Probe fractional baryon content

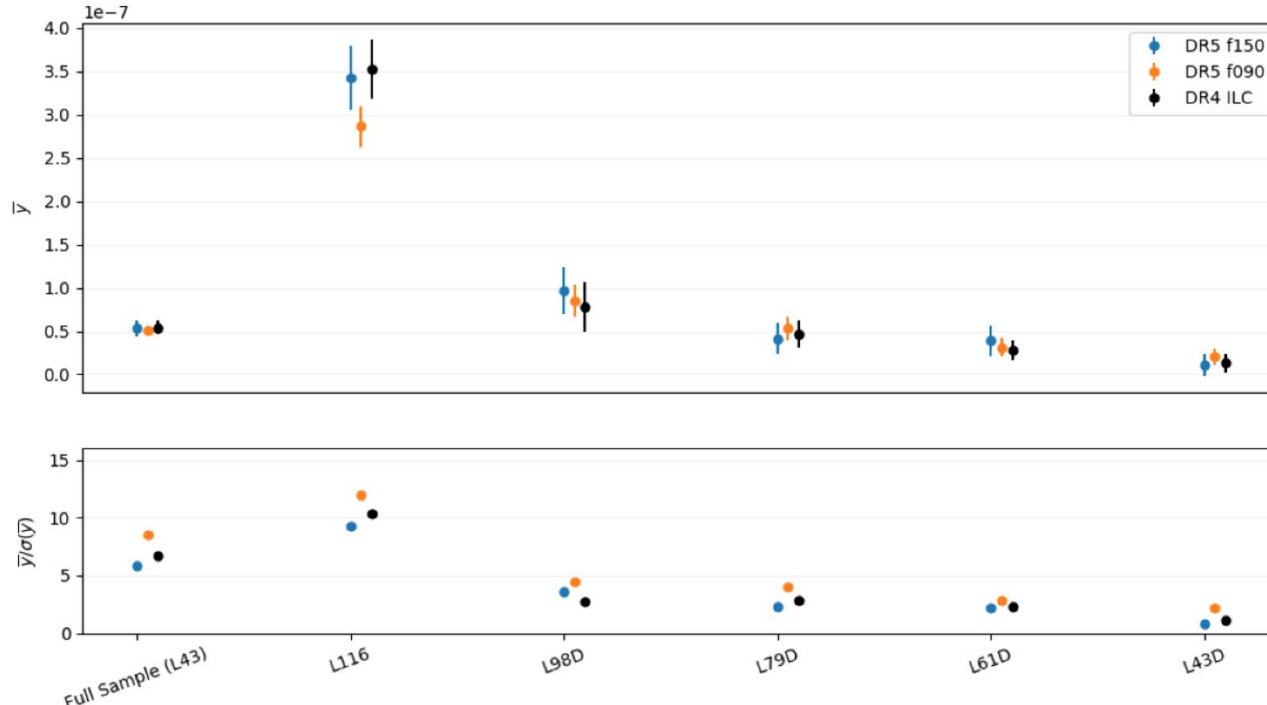


- ~1,200 sq. deg. of DES-Y1 redMaPPer data overlapping with the SPT-SZ survey
- 6,693 sources with photometric redshifts  $0.1 < z < 0.8$
- Matched filter
- $\tau \sim (3.75 \pm 0.89) \times 10^{-3}$ ,  $4.2\sigma$
- Probe gas fraction



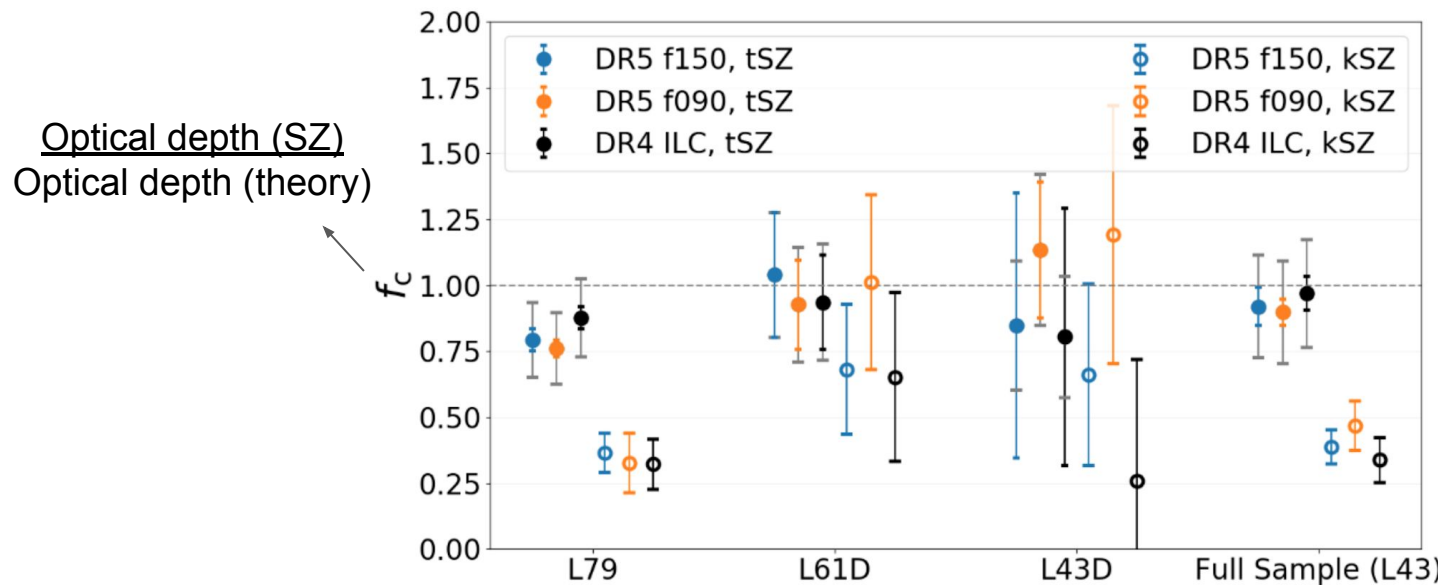
# tSZ stacking with ACT, Planck, SDSS

- Average Compton-y in 2.1' aperture from tSZ stacking with same AP filter used for pairwise kSZ
- Measurements consistent across three maps analyzed
- Higher S/N (up to 12 sigma) in higher L bins as expected



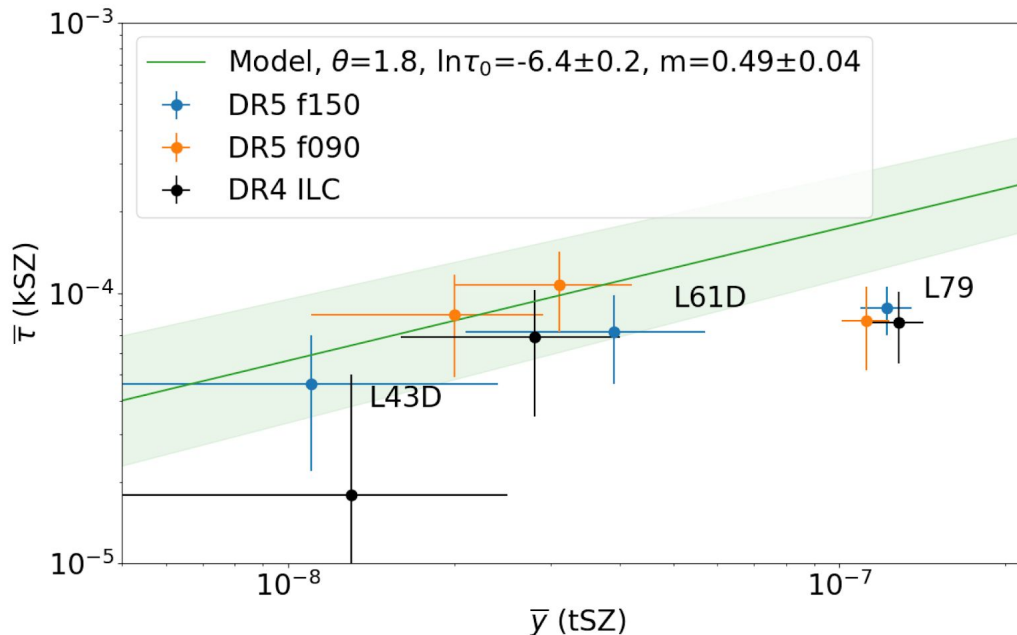
# Optical depth comparisons

- “Theoretical tau” estimated for case in which baryons trace dark matter
- kSZ and tSZ results agree within  $1\sigma$  in two bins and differ at  $2-3\sigma$  in the highest S/N bin
- Estimates from the SZ effects account for  $\frac{1}{3}$  to all of the theoretically predicted baryon content



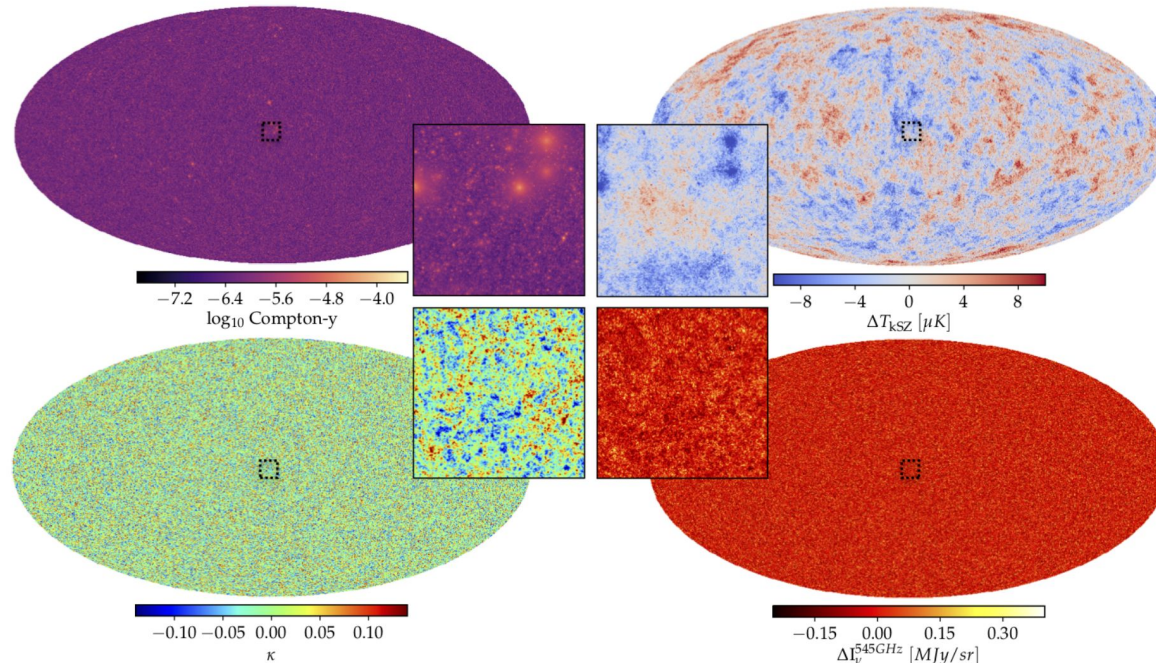
# Optical depth comparisons

- Working towards empirical  $y$ -tau relationship from tSZ and kSZ measurements
- Results are consistent with the hydrodynamical sim model in two bins, while the kSZ results in the highest L bin fall below the model line



# Future

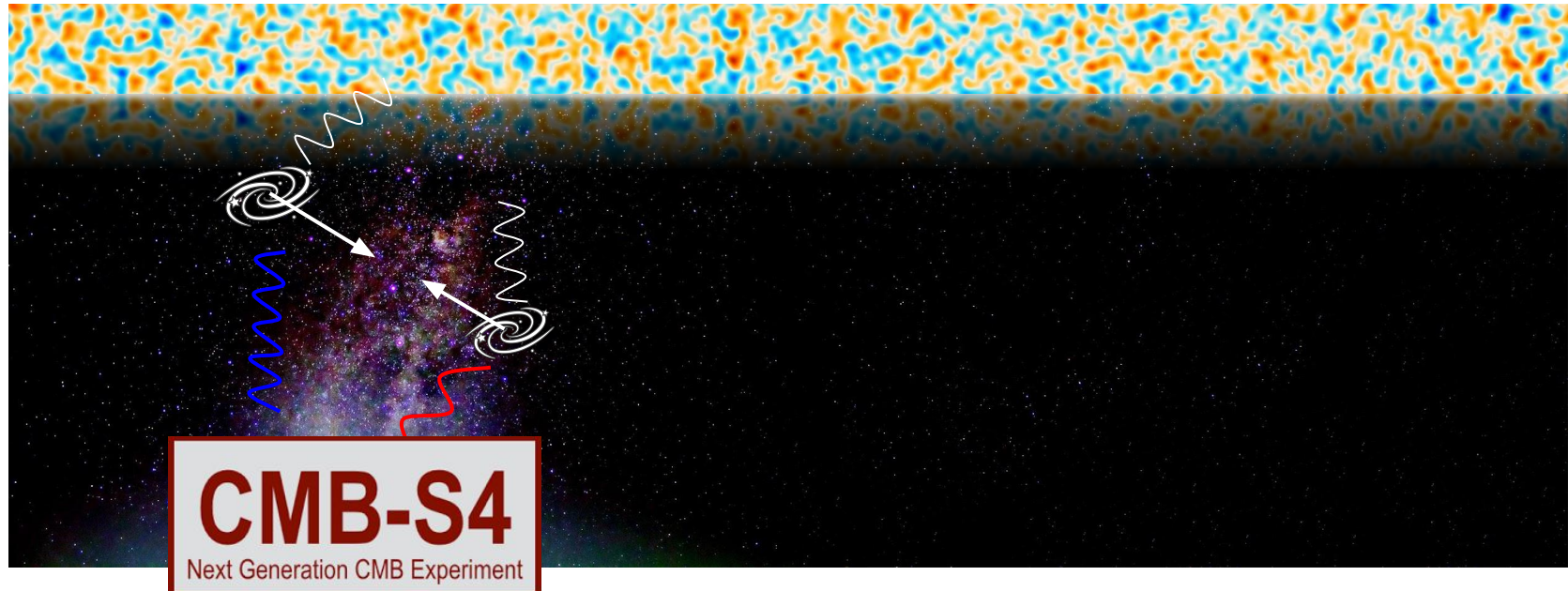
- Testing ACT pipeline on Websky simulations
- Exploring SZ signal optical depth estimate agreement
- Testing MOND



Stein et al. 2020, 2001.08787

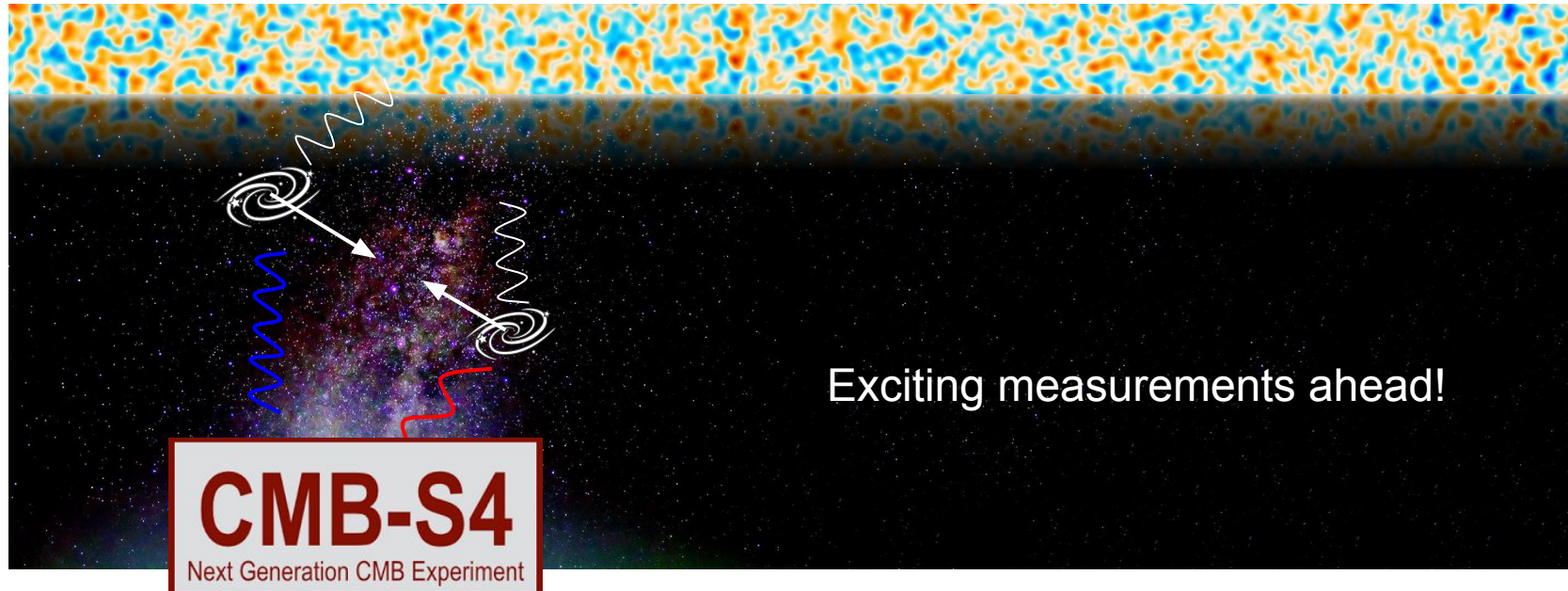
# Future

- Improve signal with deep, multifrequency data and large optical catalog overlap
- improved spectroscopic measurements: DESI, photometric measurements: Rubin/LSST
- Understand dust contamination, halo miscentering, mass uncertainties, selection effects, astrophysical uncertainties
  - Realistic simulations + mock catalogs



# Future

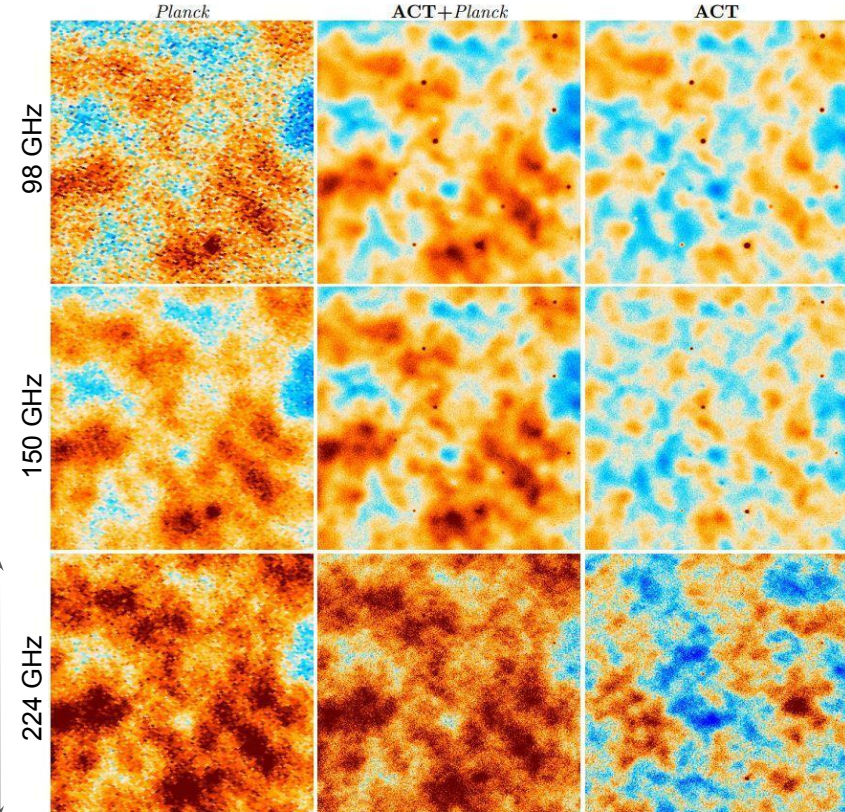
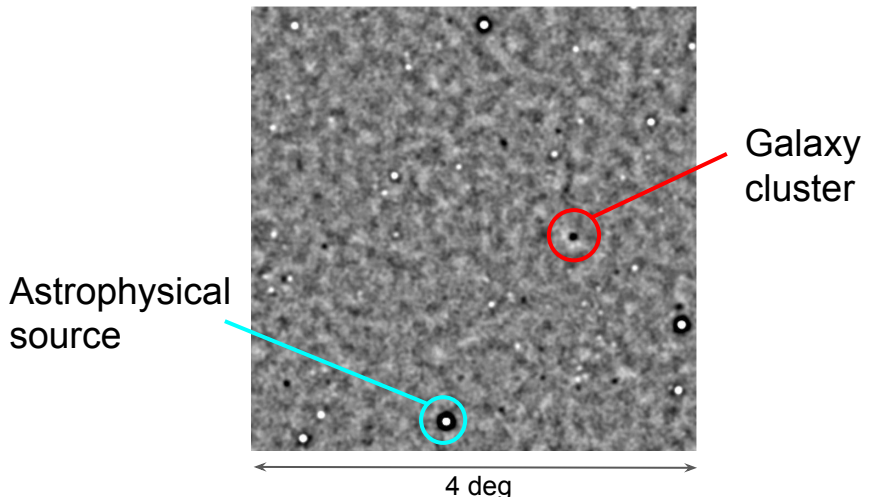
- Improve signal with deep, multifrequency data and large optical catalog overlap
- improved spectroscopic measurements: DESI, photometric measurements: Rubin/LSST
- Understand dust contamination, halo miscentering, mass uncertainties, selection effects, astrophysical uncertainties
  - Realistic simulations + mock catalogs



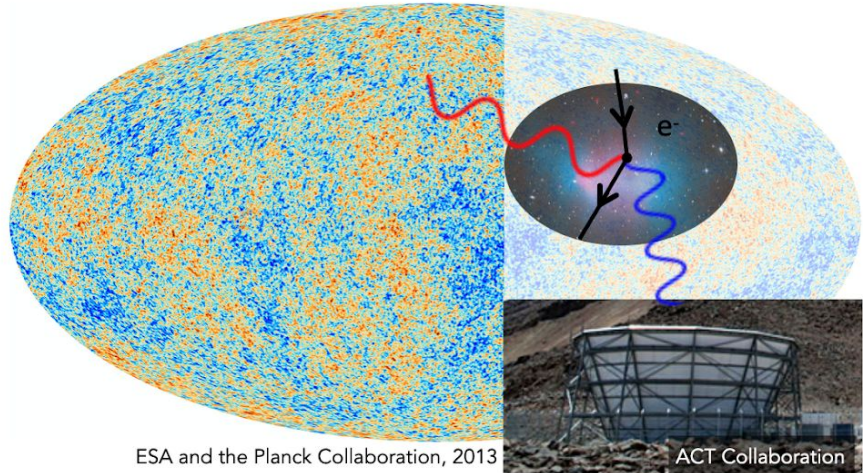
# Backup

# Secondary Anisotropies

- Imprinted after the surface of last scattering
- Contain information about evolution of the universe and intervening matter
- Can be foregrounds for primary anisotropy measurements or be studied in their own right



# The Sunyaev Zel'dovich Effects



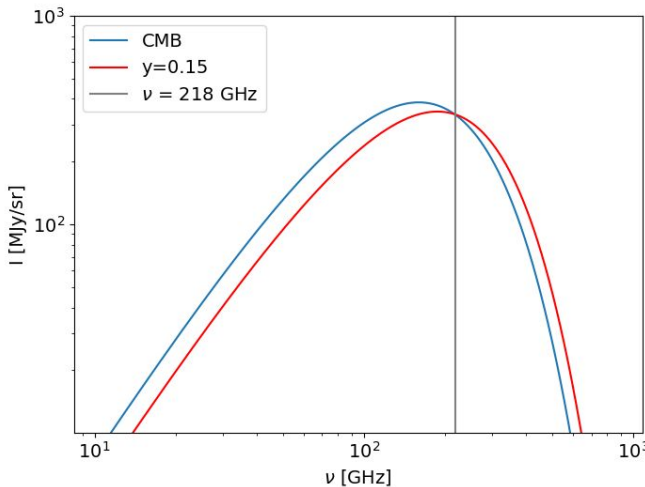
- Thermal SZ effect  
(tSZ):  $\Delta T \propto$  integrated electron pressure

$$\frac{\Delta T(\nu)}{T_{\text{CMB}}} = f(\nu)y$$

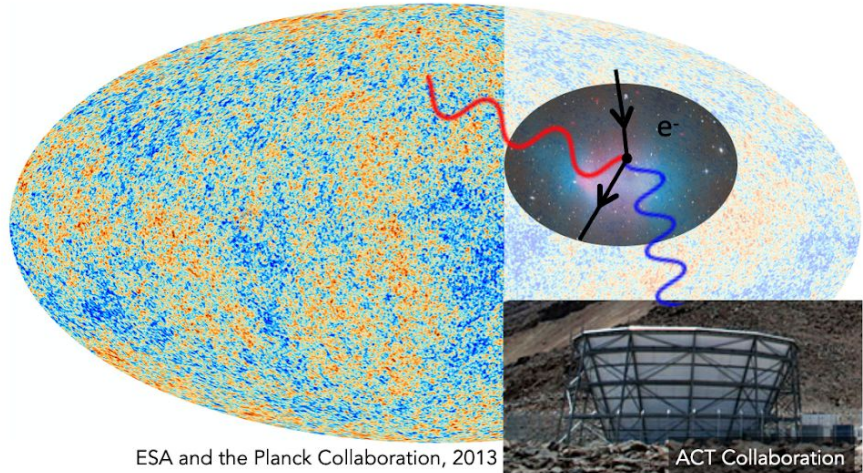
Compton-y

$$y = \frac{\sigma_T}{m_e c^2} \int_{\text{LOS}} n_e k T_e dl \quad \leftarrow \text{Number of scatterings} \times \text{energy gain/scattering}$$

**Both SZ effects  $\propto$  halo optical depth ( $\tau$ )**  $\tau = \sigma_T \int_{\text{LOS}} n_e dl$



# The Sunyaev Zel'dovich Effects

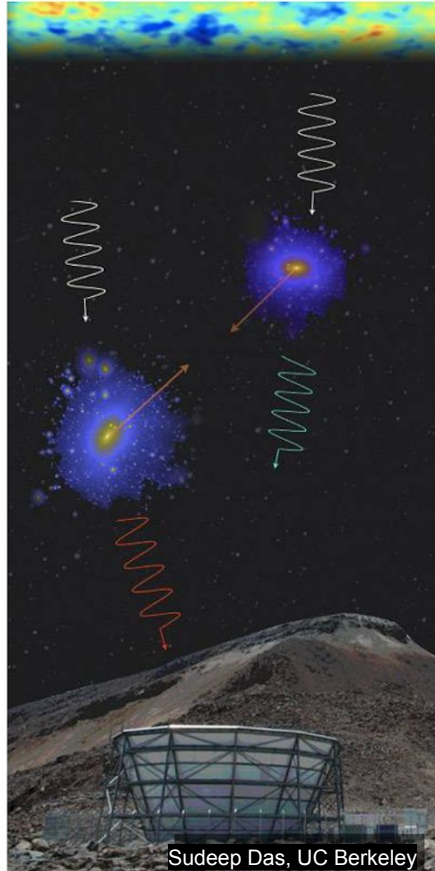


- Thermal SZ effect  
(tSZ):  $\Delta T \propto$  integrated electron pressure
- Kinematic SZ effect  
(kSZ):  $\Delta T \propto$  line of sight momentum

$$\frac{\delta T_{\text{kSZ}}(\hat{n})}{T_{\text{CMB}}} = -\tau_{\text{gal}} \left( \frac{v_{e,r}}{c} \right)$$

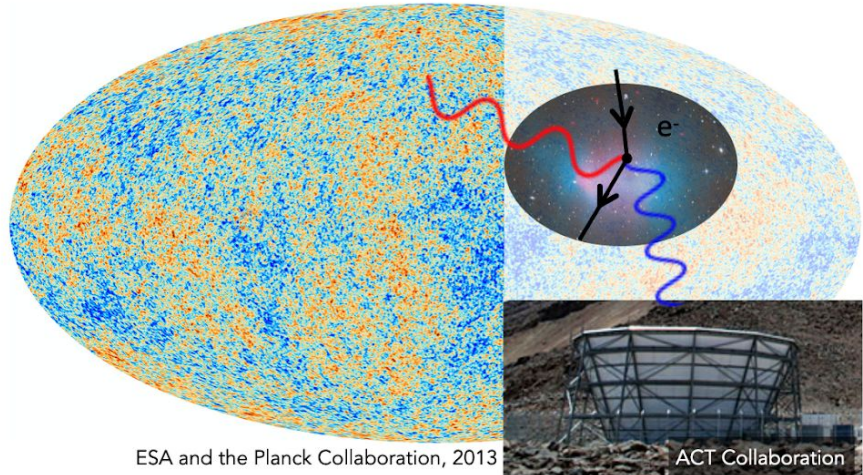
Bulk electron LOS velocity  
↓

$$\tau = \sigma_T \int_{\text{LOS}} n_e dl$$



**Both SZ effects  $\propto$  halo optical depth ( $\tau$ )**

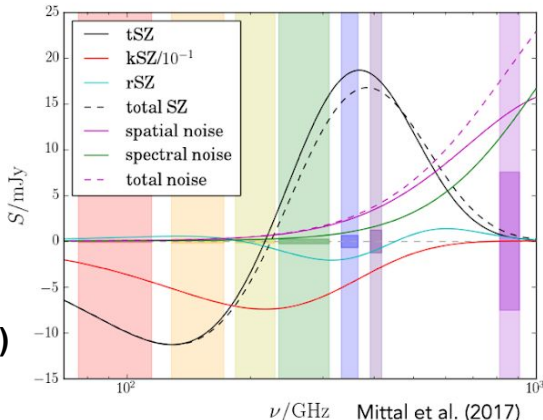
# The Sunyaev Zel'dovich Effects



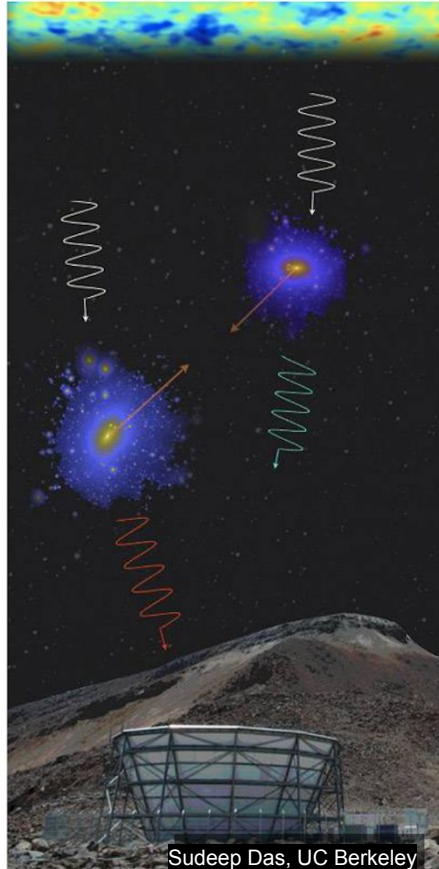
ESA and the Planck Collaboration, 2013

ACT Collaboration

- Thermal SZ effect  
(tSZ):  $\Delta T \propto$  integrated electron pressure
- Kinematic SZ effect  
(kSZ):  $\Delta T \propto$  line of sight momentum



**Both SZ effects  $\propto$  halo optical depth ( $\tau$ )**



Sudeep Das, UC Berkeley

# Dark Energy

- Potential explanation of the accelerating expansion of the universe
- Probes of large scale structure sensitive to dark energy and gravity

Equation of state

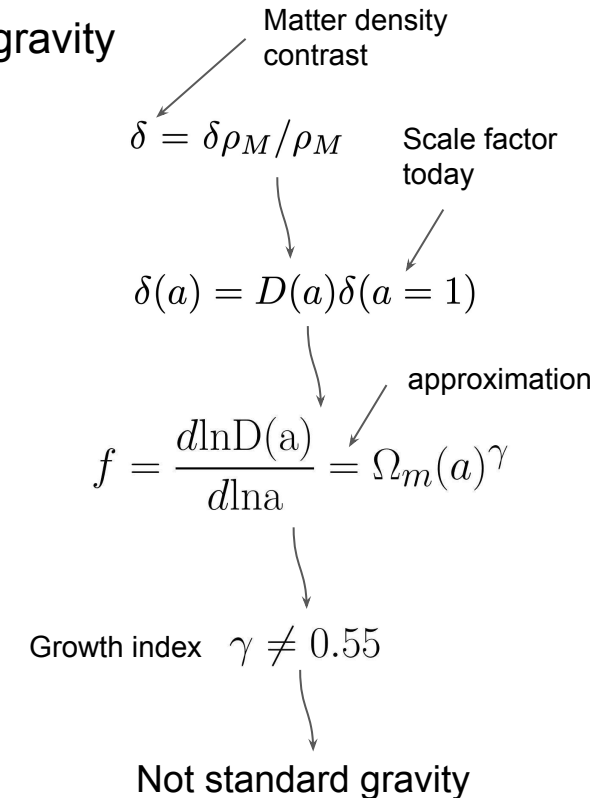
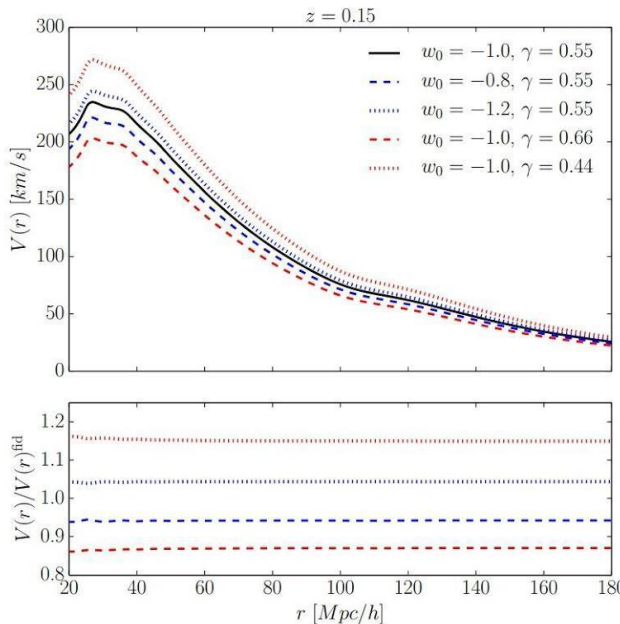
$$w = P/\rho$$

Scale factor

$$w(t) = w_0 + w_a(1 - a(t))$$

$w \neq -1, w_a \neq 0$

Not  $\Lambda$ CDM



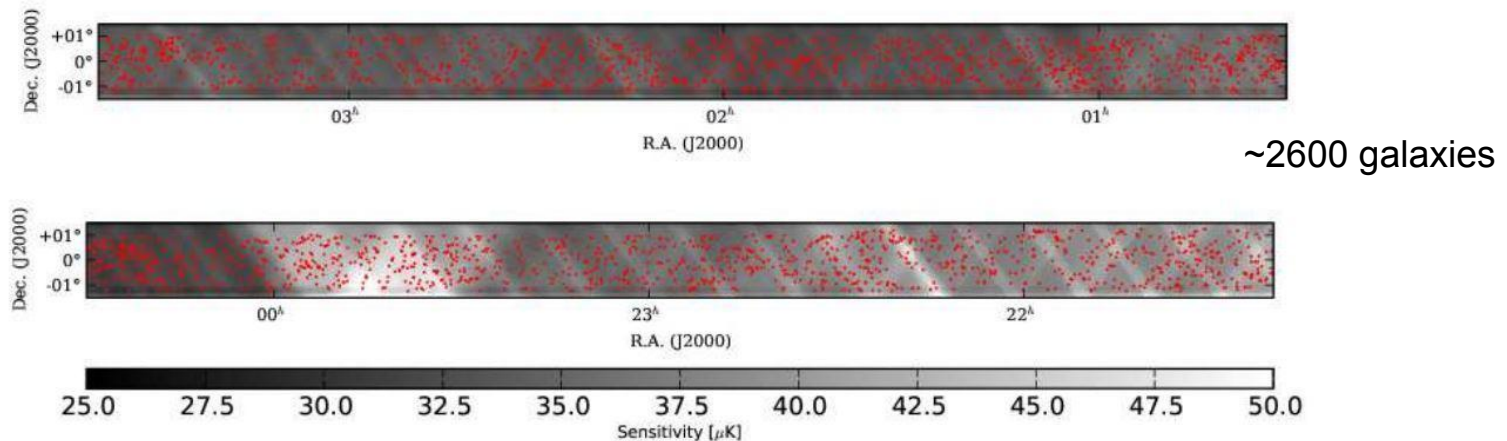
# ACT Heritage

---

- ACT, SPT, *Planck*: tSZ, kSZ measurements in CMB data
- ACT tSZ stacking and dust reconstruction:
  - B. J. Fuzia et al. (arXiv:2001.09587): *SZ-based masses and dust emission from IR-selected cluster candidates in the SHELA survey*
  - M. B. Gralla et al. (arXiv:1310.8281): *A Measurement of the Millimeter Emission and the Sunyaev-Zel'dovich Effect Associated with Low-Frequency Radio Sources*
  - T. Su et al. (arXiv:1511.06770): *On the redshift distribution and physical properties of ACT-selected DSFGs*

# ACT Heritage

- ACT tSZ/pairwise kSZ:
  - N. Hand et al. 2011 (arXiv:1101.1951): *Detection of Sunyaev-Zel'dovich Decrement in Groups and Clusters Associated with Luminous Red Galaxies*
    - Matched-filtered map, tSZ stacking



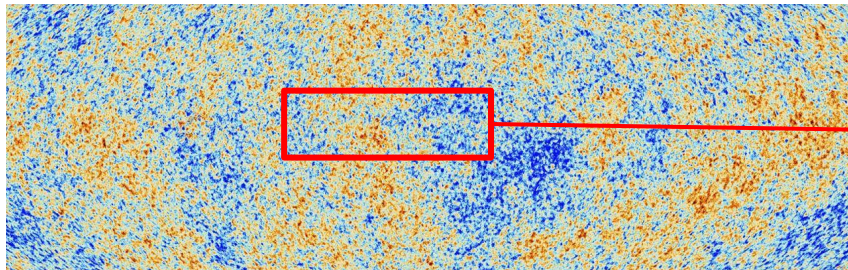
# ACT Contemporary

---

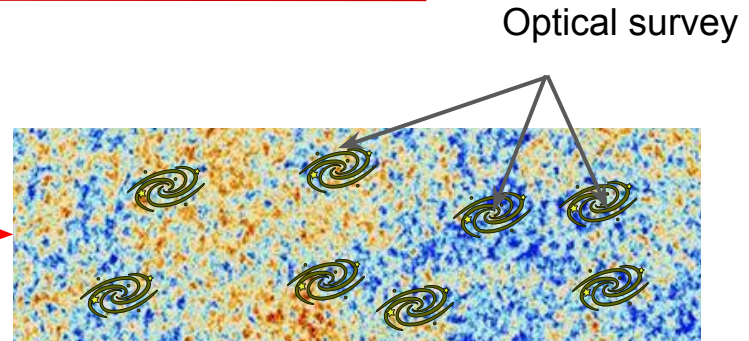
- E. Schaan et al. 2021 (arXiv:2009.05557): *The Atacama Cosmology Telescope: Combined kinematic and thermal Sunyaev-Zel'dovich measurements from BOSS CMASS and LOWZ halos*
  - tSZ measurements and velocity reconstruction kSZ estimator with same coadded ACT+*Planck* maps, CMASS + LOWZ BOSS galaxies
- S. Amodeo et al. 2021 (arXiv:2009.05558): *The Atacama Cosmology Telescope: Modeling the Gas Thermodynamics in BOSS CMASS galaxies from Kinematic and Thermal Sunyaev-Zel'dovich Measurements*
  - Constraints on gas thermodynamics of CMASS galaxies with tSZ and kSZ measurements

# Measurement principles

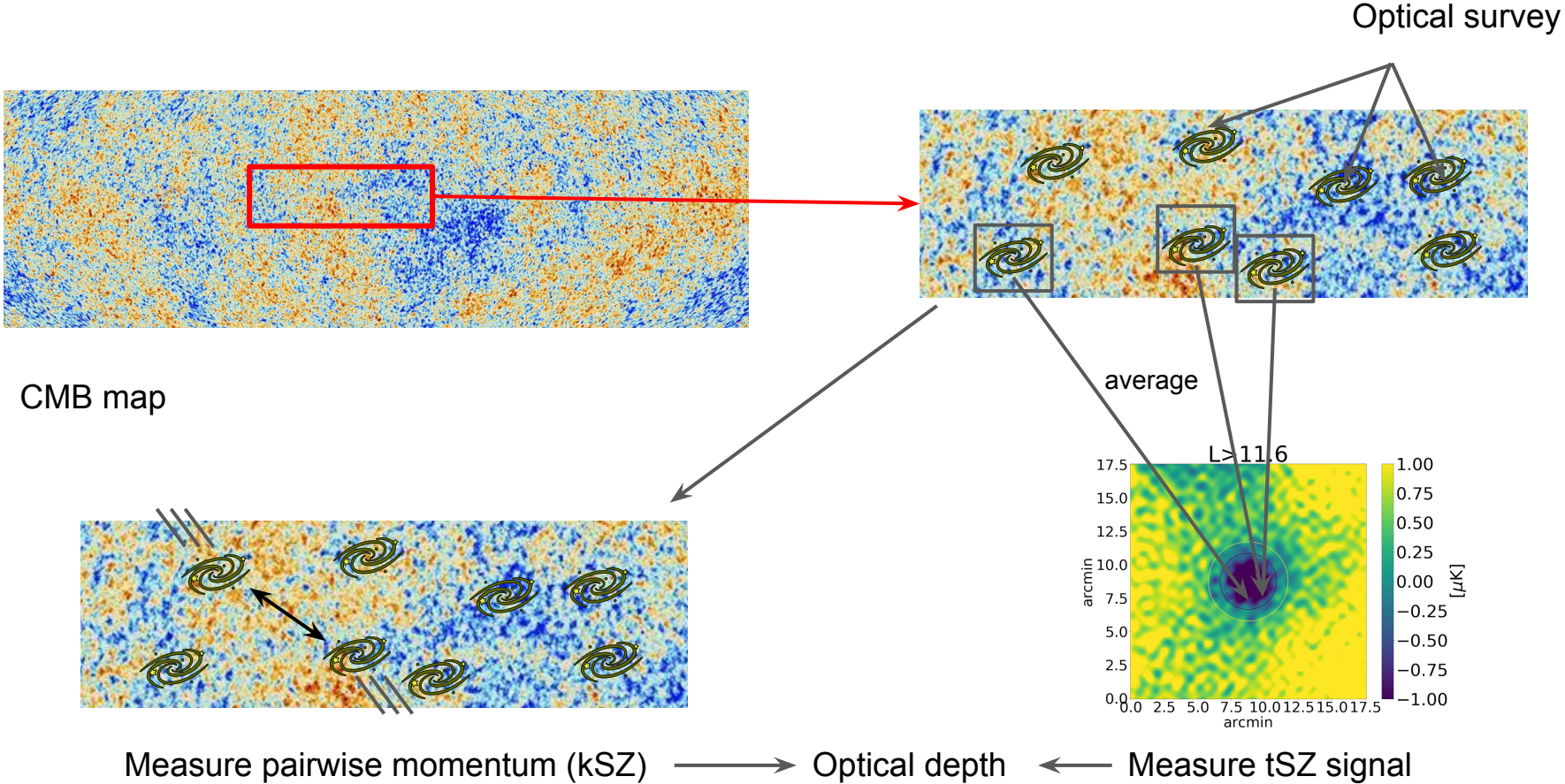
---



CMB map

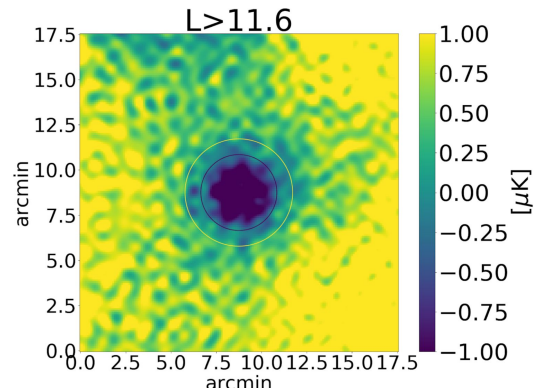


# Measurement principles



# Optical depth from tSZ measurements

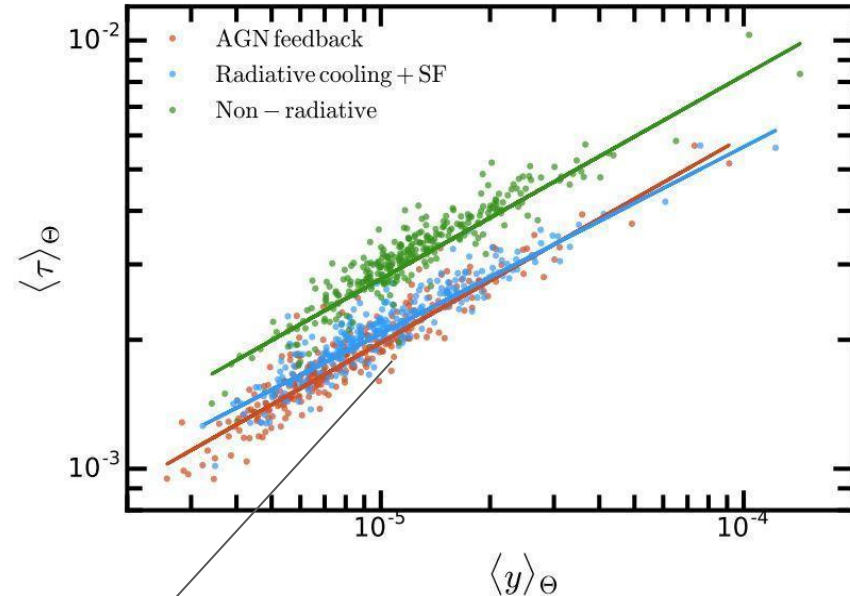
- Simulations of galaxy evolution provide relationship between Compton-y and optical depth



Measurement: either in  
temperature or Compton-y

$$\frac{\Delta T(\nu)}{T_{\text{CMB}}} = f(\nu)y$$

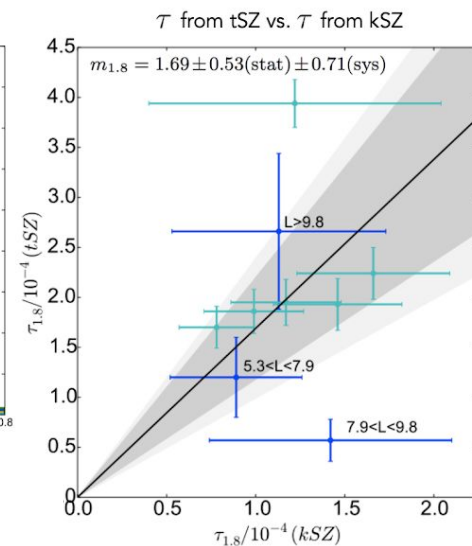
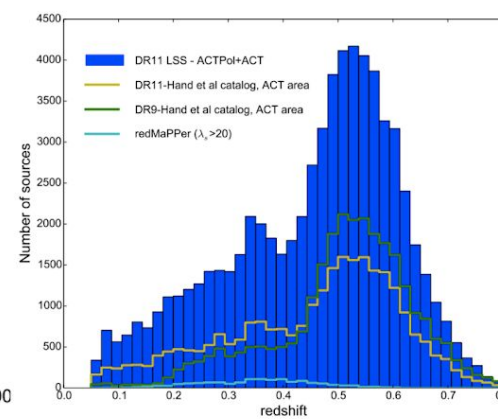
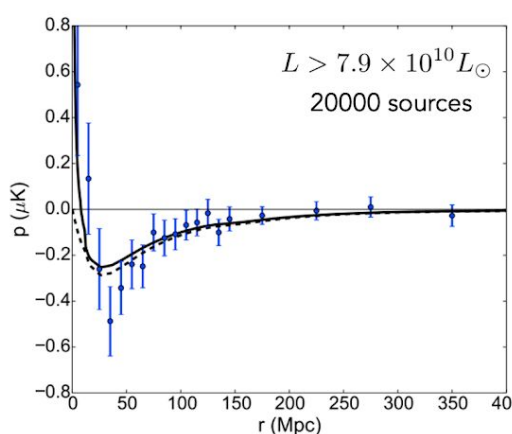
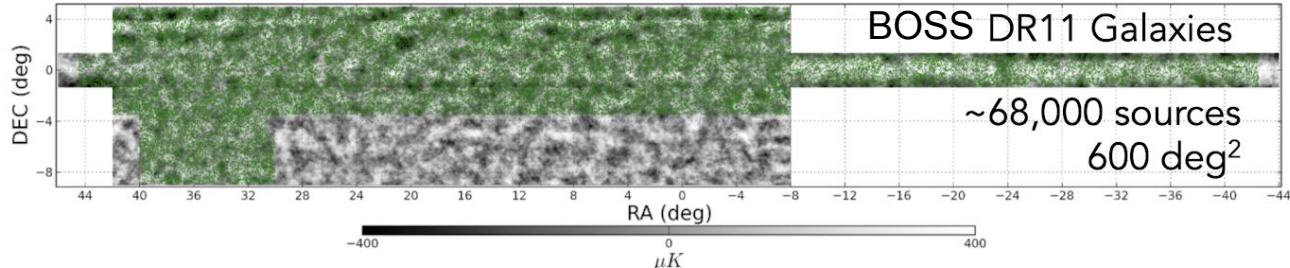
Compton-y → Optical depth  $\tau$



Battaglia (2017) 1607.02442

# ACT DR3 and SDSS DR11

- $4\sigma$  measurement of kSZ effect over a range of luminosity cuts
- Optical depth estimates from kSZ and tSZ consistent



# ACT+Planck coadded maps (DR 5)

- 2008-2018 ACT data
- 2015 & 2018 *Planck* data
- 100, 150, 220 GHz
- 4,000 SZ clusters, 18500 point source candidates

Publicly available:  
[https://lambda.gsfc.nasa.gov/  
product/act/actpol\\_prod\\_table.cfm](https://lambda.gsfc.nasa.gov/product/act/actpol_prod_table.cfm)

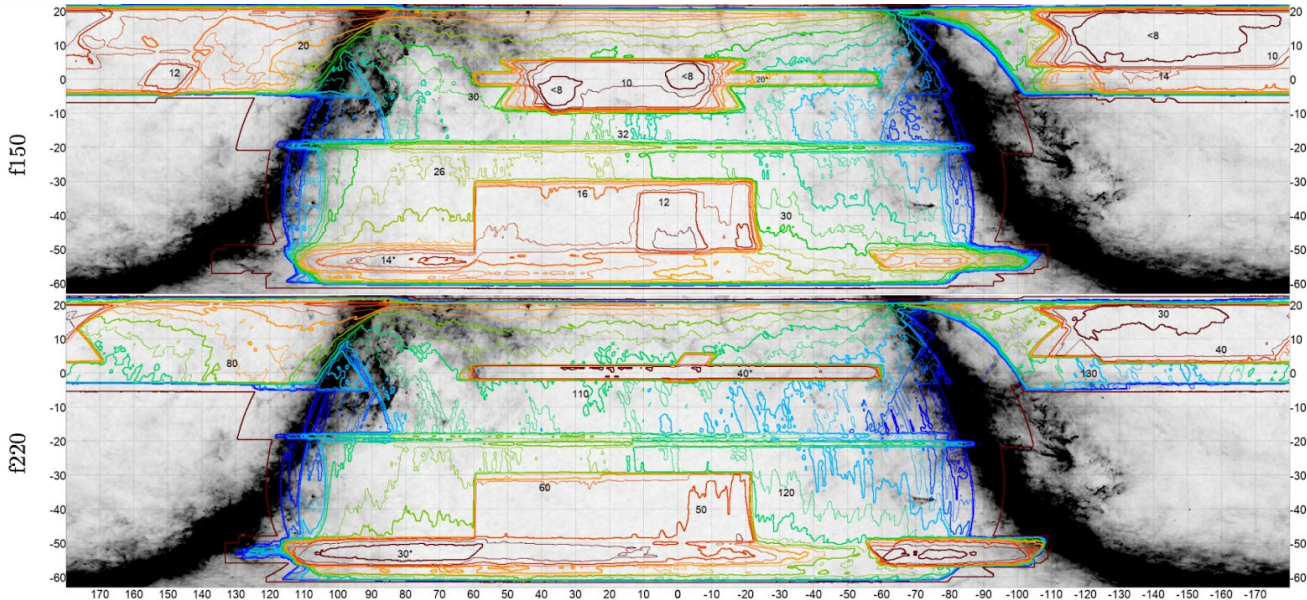


Figure 15: Spatial distribution of ACT-only map depths for the three different ACT frequencies, as shown by iso-depth contours that go from 8/8/30  $\mu\text{K}$ -arcmin (red) to 60/50/180  $\mu\text{K}$ -arcmin (blue) with contour intervals of 2/2/10  $\mu\text{K}$ -arcmin for f090/f150/f220 respectively. This covers most of the depth range in the maps, though there are areas that are somewhat deeper or shallower. The outermost red curve shows the full outline of the survey area. Selected contour lines are labeled with their depth to make it easier to read off values. These are T noise levels; Q and U are approximately  $\sqrt{2}$  higher. They also only describe the noise level at small scales. The background grayscale map is the dust-dominated *Planck* 353 GHz map.

# Component separated maps (DR 4)

- Component separated maps with internal linear combination approach
- ACT and *Planck* data
- Compton-y, CMB+kSZ

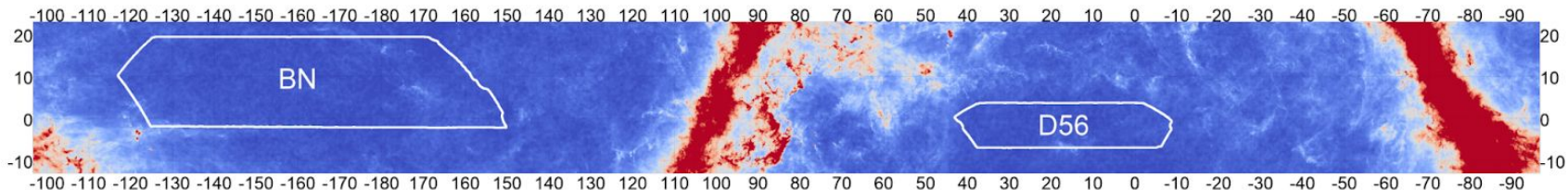


FIG. 3: Sky regions analyzed in this work. The vertical axis (declination) and horizontal axis (right ascension) are labeled in degrees. The BN region (1633 sq. deg) and D56 region (456 sq. deg.) that we analyze are labeled. The background shows the *Planck* 353 GHz temperature map in this sky region.

M. Madhavacheril et al. 2020, PRD (1911.05717)

# ACT DR4, DR5 and SDSS DR15

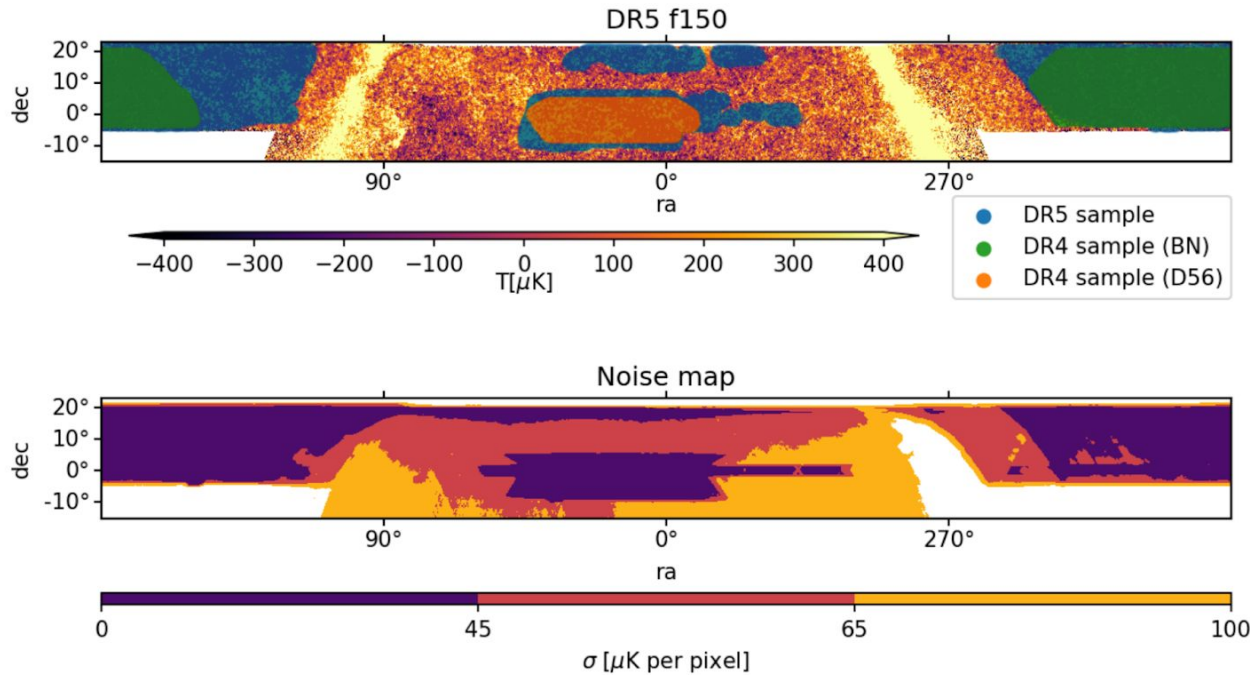
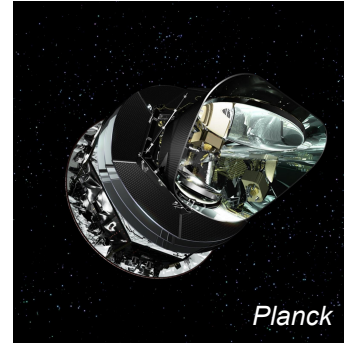
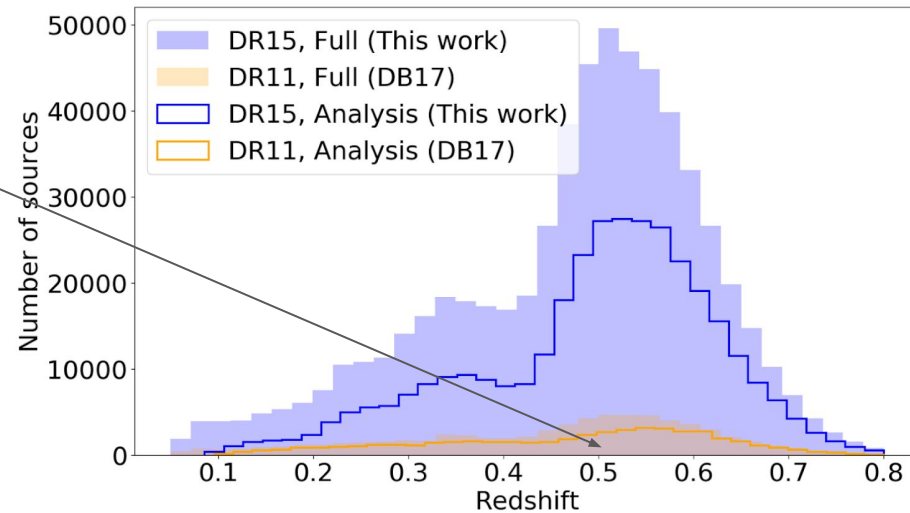
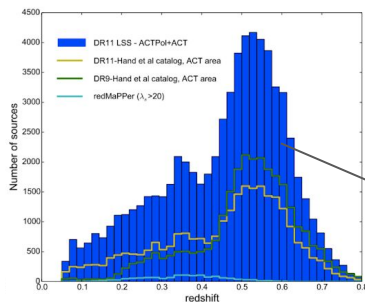


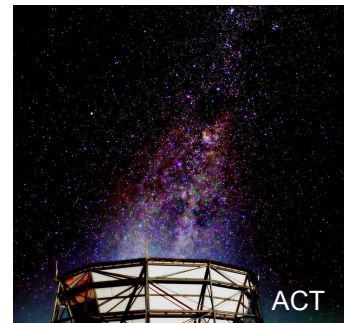
FIG. 1: Top: The ACT + *Planck* map used for the DR5 f150 analysis with the overlapping 343,647 SDSS DR15 selected sources plotted in blue over 3,700 sq. deg., and the BN and D56 areas covered by the ILC maps plotted in green and orange, respectively. Bottom: The inverse white noise variance map associated with the DR5 f150 coadded ACT+*Planck* map highlighting regions representing a noise equivalence of 45 and 65  $\mu\text{K}$  per pixel (with a 0.5 arcmin resolution plate Carré projection), which were used to cut the SDSS sample for the DR5 f150 analysis. The orange and yellow regions of higher noise overlapped with 27% of the DR15 sample. Results are shown for the more conservative 45  $\mu\text{K}$  per pixel inverse white noise variance map cut, shown in purple. We performed an equivalent cut for the DR5 f090 map and analysis.

# ACT DR4, DR5 and SDSS DR15

- ACT+*Planck* coadded maps: 150, 98 GHz
- Component separated maps of Compton-y, CMB+kSZ
- BOSS-SDSS DR15 galaxies as proxies for group centers
  - Larger area with more optical source overlap: 3,700 sq. deg. and 343,647 sources



Planck



ACT



Sloan Foundation Telescope

# SDSS DR15 Binning

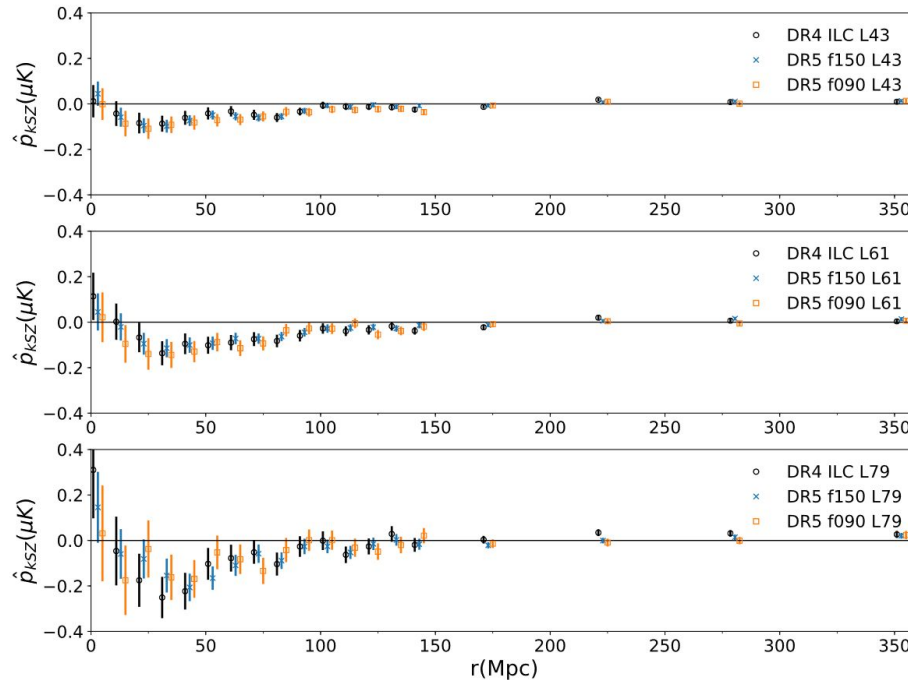
---

- 5 cumulative, 5 disjoint luminosity bins
- Cuts chosen based off 2017 work
- 3 equally-spaced bins selected for joint analysis (kSZ and tSZ)
- Cut based on a point source mask, galactic plane mask, CMB noise level cut

Bin	Luminosity cut/ $10^{10} L_{\odot}$	$M_{\text{vir}}$ cut/ $10^{13} M_{\odot}$	$\langle M_* \rangle / 10^{11} M_{\odot}$	DR5 f150, DR5 f090			DR4 ILC		
				N	$\langle L \rangle / 10^{10} L_{\odot}$	$\langle z \rangle$	N	$\langle L \rangle / 10^{10} L_{\odot}$	$\langle z \rangle$
L43*	$L > 4.30$	$M > 0.52$	2.21	343647	7.4	0.49	190551	7.4	0.50
L61*	$L > 6.10$	$M > 1.00$	2.61	213070	8.7	0.51	118852	8.7	0.51
L79*	$L > 7.90$	$M > 1.66$	3.17	103159	10.6	0.53	57828	10.6	0.54
L98	$L > 9.80$	$M > 2.59$	3.84	46956	12.8	0.56	26308	12.8	0.57
L116	$L > 11.60$	$M > 3.70$	4.50	23504	15.0	0.58	13277	15.0	0.59
L43D*	$4.30 < L < 6.10$	$0.52 < M < 1.00$	1.57	130577	5.2	0.48	71699	5.2	0.48
L61D*	$6.10 < L < 7.90$	$1.00 < M < 1.66$	2.08	109911	6.9	0.48	61024	6.9	0.48
L79D	$7.90 < L < 9.80$	$1.66 < M < 2.59$	2.61	56203	8.7	0.51	31520	8.7	0.52
L98D	$9.8 < L < 11.60$	$2.59 < M < 3.70$	3.18	23452	10.6	0.54	13031	10.6	0.55

# Pairwise kSZ

- High luminosity cut -> more massive galaxies, higher signal
- Higher luminosity cut -> lower galaxy count -> larger uncertainty



L43 -> lum > 4.3e10 Lsun

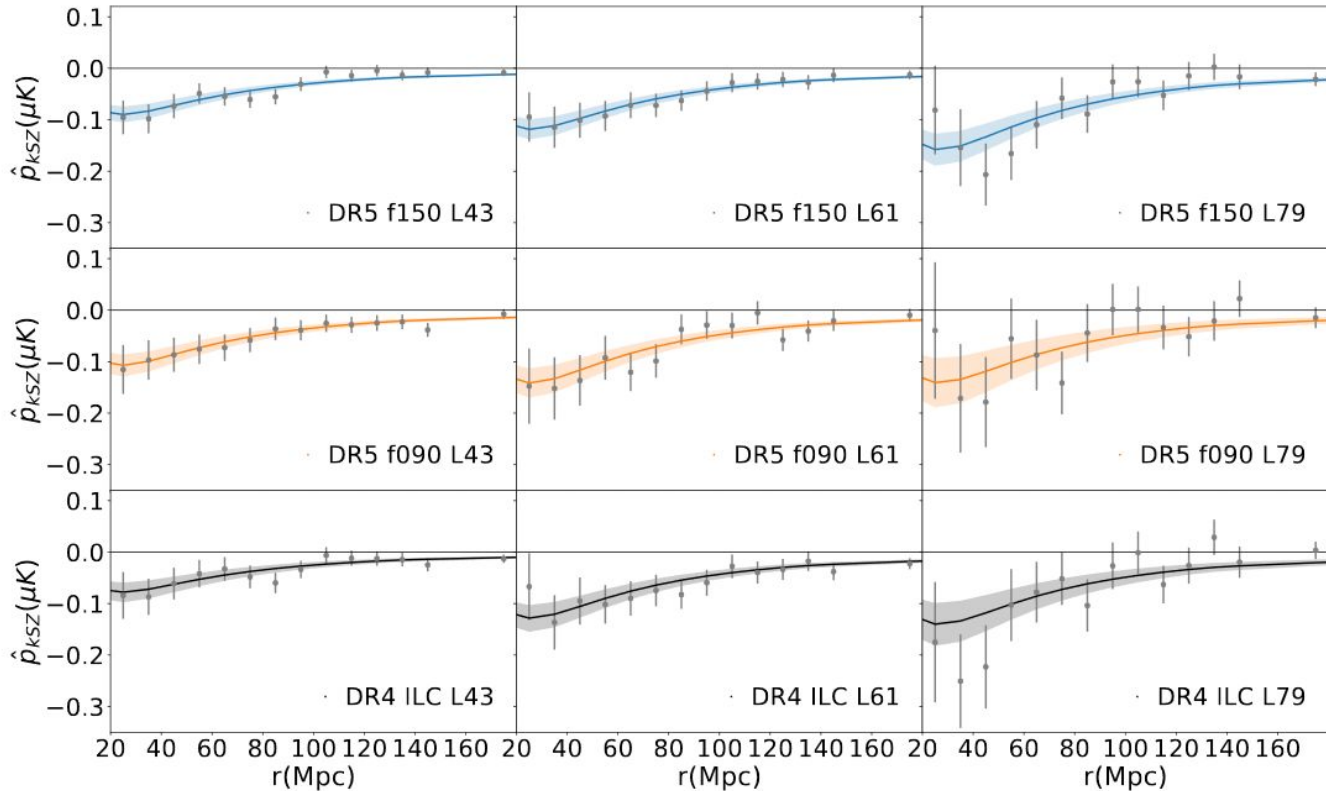
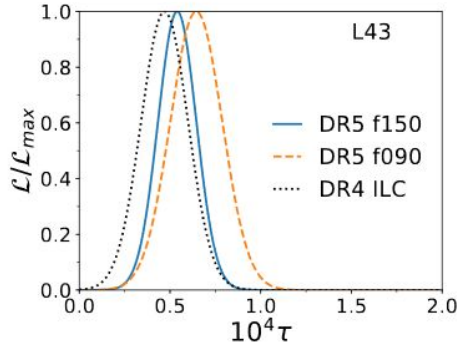
L61 -> lum > 6.1e10 Lsun

L79 -> lum > 7.9e10 Lsun

# Pairwise kSZ results

$$\hat{p}_{\text{th}}(r, z) = -\frac{T_{CMB}}{c} \bar{\tau} V(r, z)$$

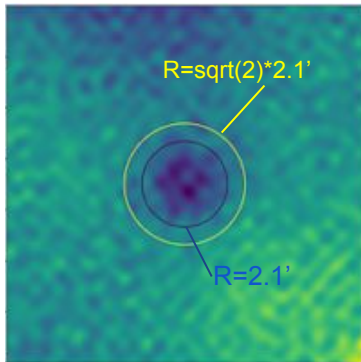
- **5.4 sigma detection**
- Fits to model yield estimate of optical depth
- Consistent across maps



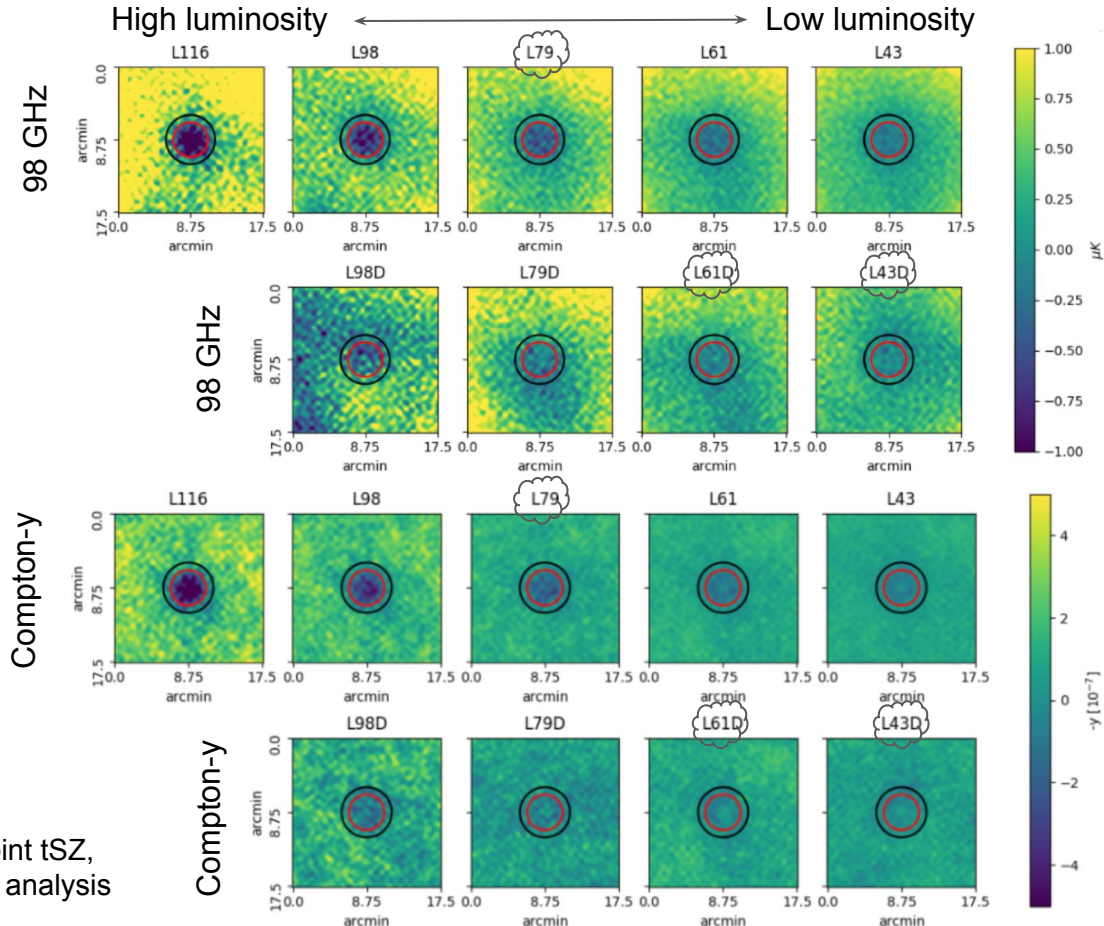
# tSZ stacking

- Galaxy-centered submaps
- Aperture photometry with 2.1' radius aperture (same as kSZ)
- Jackknife error bar estimates

$$\delta T_i = T_{\text{disk}} - T_{\text{ring}}$$



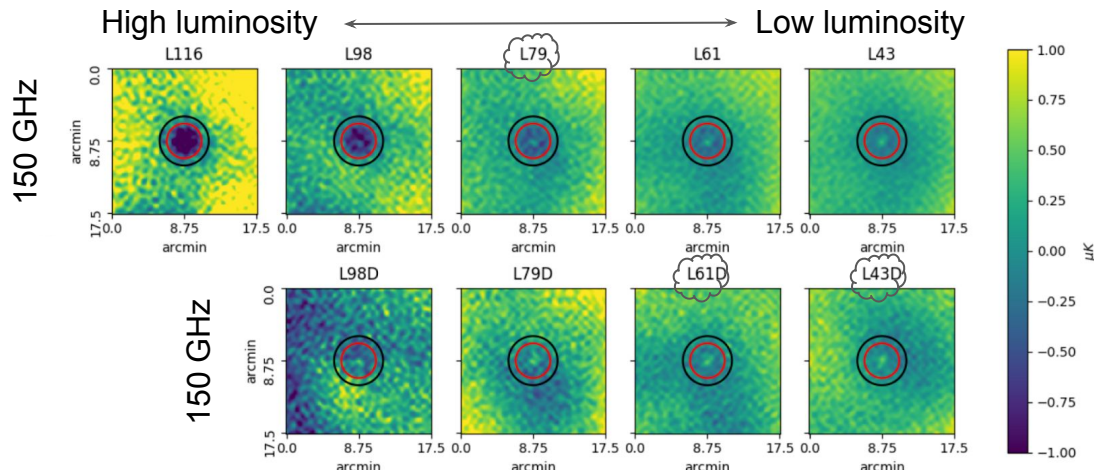
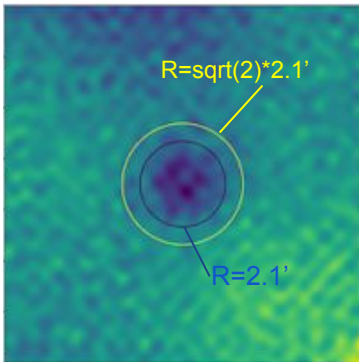
= Joint tSZ,  
kSZ analysis



# tSZ stacking

- Galaxy-centered submaps
- Aperture photometry with 2.1' radius aperture (same as kSZ)
- Jackknife error bar estimates

$$\delta T_i = T_{\text{disk}} - T_{\text{ring}}$$



Central “bright spot” from dust emission

= Joint tSZ,  
kSZ analysis

# tSZ stacking

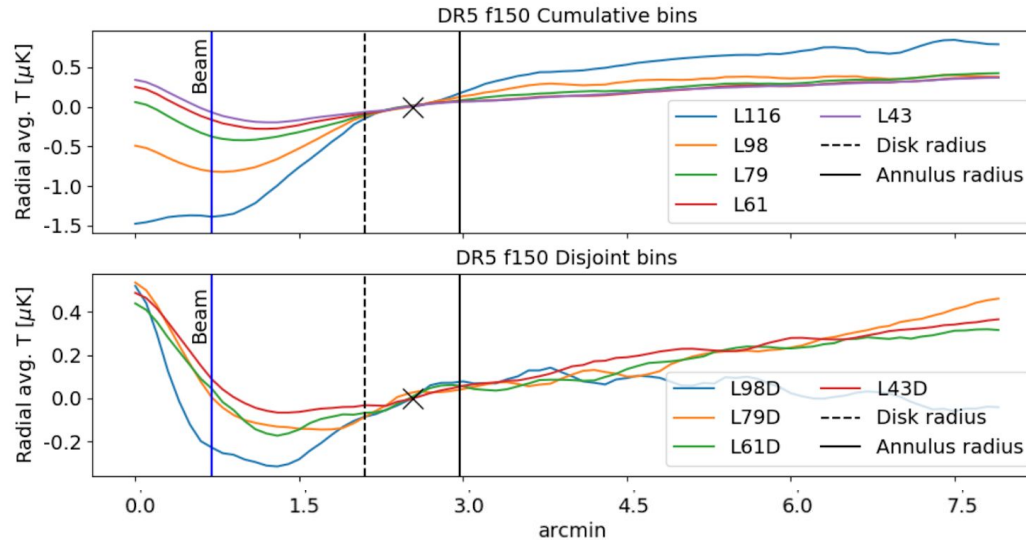


FIG. 4: Radial average of the stacked submaps, which have been repixelized to  $0.1'$  per pixel, normalized to the average annulus value (as shown with plotted crosses), for each luminosity bin, for the DR5 f150 and DR5 f090 coadded maps as well as the DR4 ILC map, shown for illustrative purposes only. The native units of the DR5 f150 and DR5 f090 maps are in  $\mu\text{K}$  and the DR4 ILC maps in  $y$ . Negative  $y$  is plotted here to compare with the decrements present in temperature. The aperture photometry disk radius is plotted as a vertical black dashed line, and the annulus outer radius is plotted as a vertical solid black line. The beam radius is plotted as a blue vertical line for DR5 f150, an orange vertical line for DR5 f090, and a black vertical line for the effective DR4 ILC beam. A central ‘bright spot’ is observed in nearly all but the most luminous bin, and is attributed to dust emission. Due to this effect, we studied the core-excised AP approach for the DR5 f150 and DR5 f090 analysis (Sections III.B, III.C).

# tSZ results

- Measurements consistent across frequencies
- Herschel data used for dust contamination correction (Amodeo et al. 2020, arXiv:2009.05558)

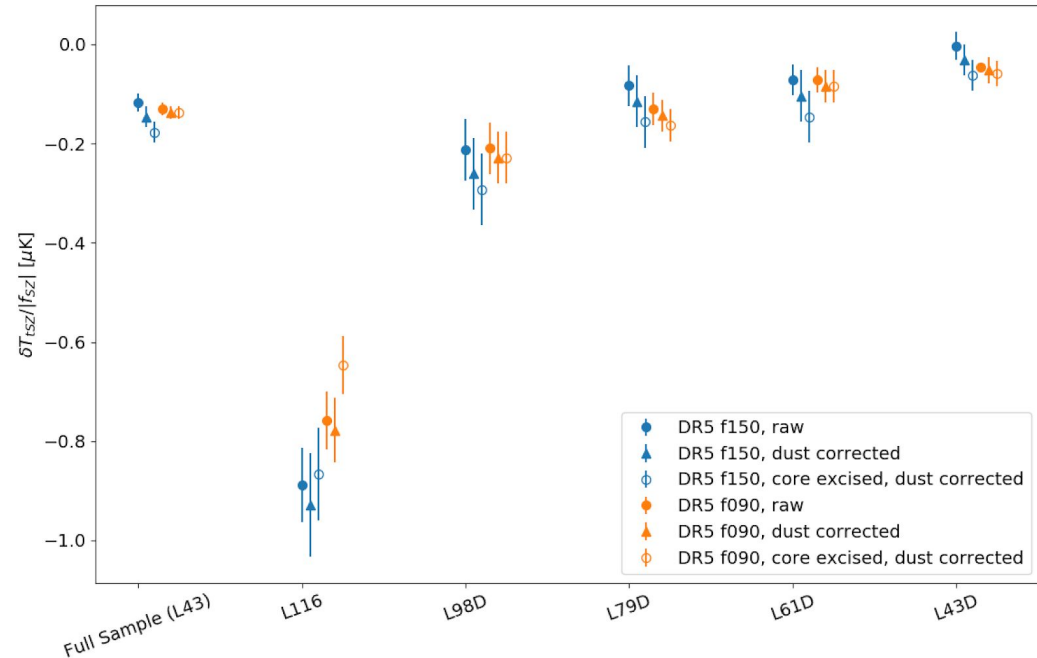
simulations to infer the optical depth [3]. To obtain the Compton- $y$  parameter we follow the steps detailed in [18] and DB17. The tSZ temperature signal is related to the Compton- $y$  parameter by

$$\frac{\delta T_{\text{tSZ}}(\theta)}{T_{\text{CMB}}} = f_{\text{SZ}} y(\theta), \quad (1)$$

where  $y(\theta)$  is the Compton parameter at a projected angle  $\theta$  from the cluster center and, in the non-relativistic limit,  $f_{\text{SZ}}$  depends on observed radiation frequency:

$$f_{\text{SZ}} = \left( x \frac{e^x + 1}{e^x - 1} - 4 \right). \quad (2)$$

Here,  $x = h\nu/k_B T_{\text{CMB}}$  [52]. The effective band centers vary based on sky position in the coadded maps, so the

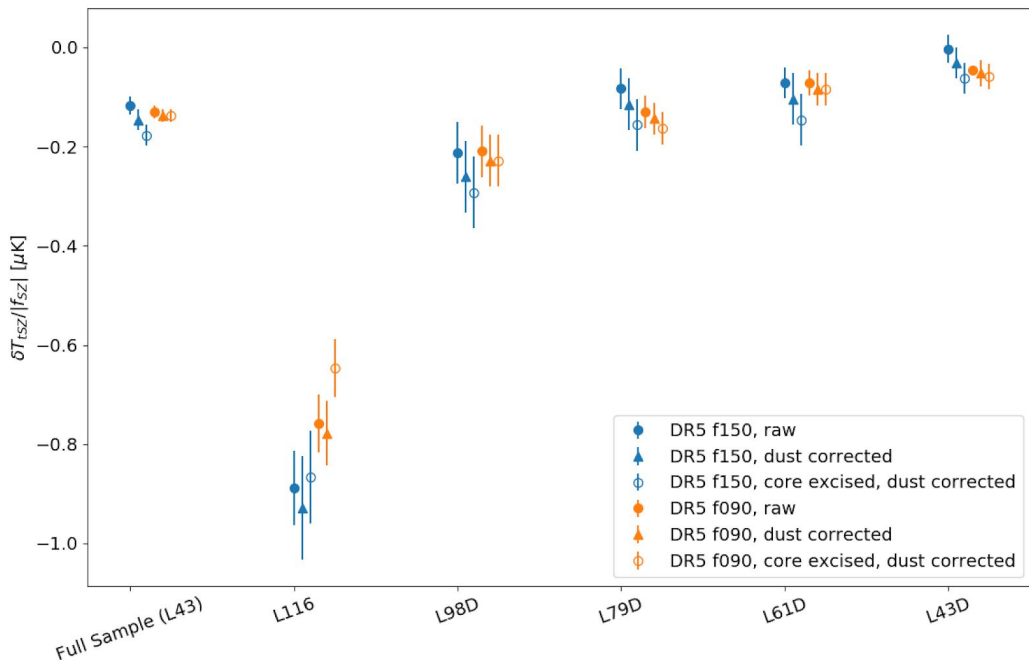


# tSZ results

- Measurements consistent across frequencies
- Herschel data used for dust contamination correction (Amodeo et al. 2020, arXiv:2009.05558)

Bin	N	$T_{\text{dust}, 150\text{GHz}} [\mu\text{K}]$	$T_{\text{dust}, 98\text{GHz}} [\mu\text{K}]$
L43	12726	$0.026^{+0.014}_{-0.008}$	$0.012^{+0.008}_{-0.004}$
L61	7784	$0.028^{+0.019}_{-0.010}$	$0.013^{+0.010}_{-0.005}$
L79	3858	$0.029^{+0.016}_{-0.010}$	$0.014^{+0.009}_{-0.005}$
L98	1795	$0.037^{+0.027}_{-0.014}$	$0.017^{+0.014}_{-0.007}$
L116	941	$0.043^{+0.063}_{-0.023}$	$0.021^{+0.031}_{-0.011}$
L43D	4872	$0.026^{+0.022}_{-0.011}$	$0.013^{+0.011}_{-0.005}$
L61D	3926	$0.034^{+0.037}_{-0.017}$	$0.018^{+0.023}_{-0.010}$
L79D	2063	$0.027^{+0.026}_{-0.012}$	$0.014^{+0.015}_{-0.007}$
L98D	854	$0.049^{+0.035}_{-0.021}$	$0.022^{+0.016}_{-0.010}$

TABLE 2: Estimated dust signal and  $1\sigma$  statistical uncertainties for the DR5 f150 and DR5 f090 maps using 4 percent of the SDSS sample used in this analysis overlapping with the *Herschel* map areas, as computed using the method described in [37].



# tSZ results

---

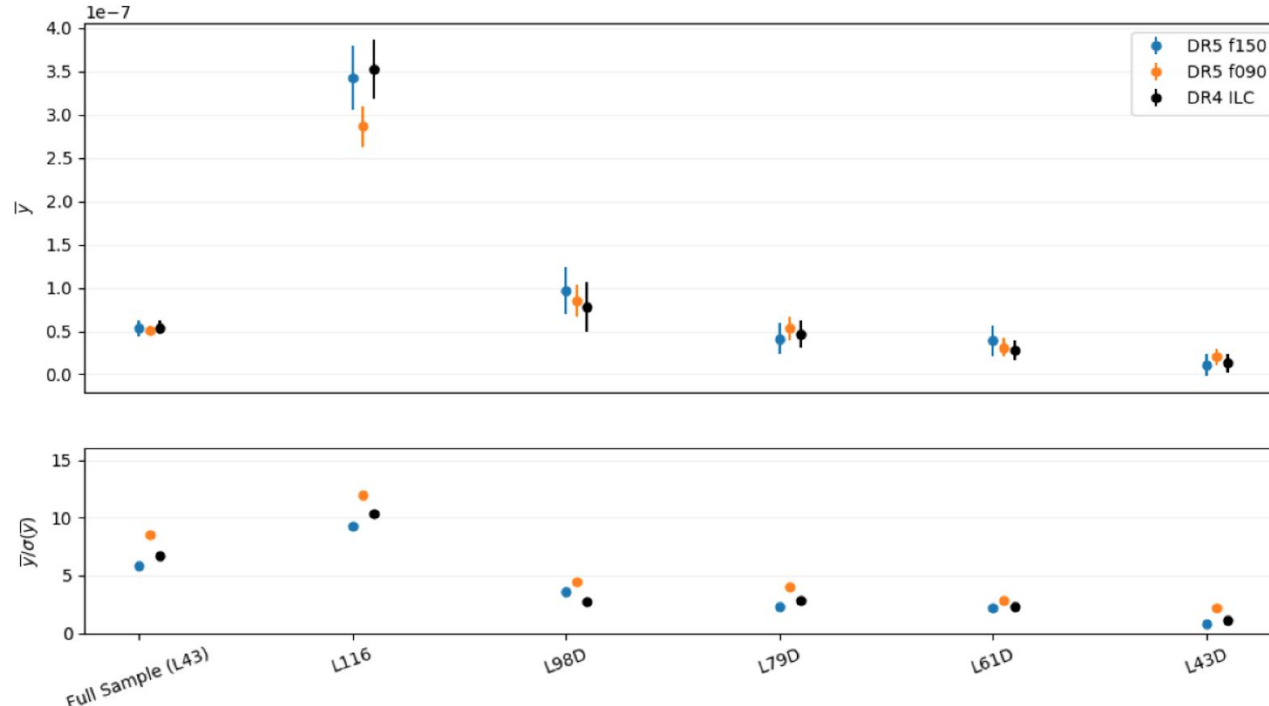
- Average Compton- $y$  in 2.1' aperture from tSZ stacking results
- Measurements consistent across three maps analyzed
- Higher S/N (up to 12 sigma) in higher L bins as expected

Bin	DR5 f150		DR5 f090		DR4 ILC
	$\delta T_{\text{tSZ,corr.}} (\mu\text{K})$	$\bar{y}/10^{-7}$	$\delta T_{\text{tSZ,corr.}} (\mu\text{K})$	$\bar{y}/10^{-7}$	$\bar{y}/10^{-7}$
L43	-0.14 ± 0.02	0.53 ± 0.09	-0.21 ± 0.02	0.51 ± 0.06	0.54 ± 0.08
L61	-0.21 ± 0.03	0.79 ± 0.11	-0.29 ± 0.03	0.70 ± 0.07	0.78 ± 0.10
L79 <sup>+</sup>	-0.32 ± 0.03	1.22 ± 0.13	-0.47 ± 0.04	1.12 ± 0.11	1.28 ± 0.14
L98	-0.57 ± 0.06	2.18 ± 0.22	-0.77 ± 0.06	1.84 ± 0.15	2.19 ± 0.21
L116	-0.89 ± 0.10	3.42 ± 0.37	-1.19 ± 0.10	2.86 ± 0.24	3.52 ± 0.32
L43D <sup>+</sup>	-0.03 ± 0.03	0.11 ± 0.13	-0.08 ± 0.04	0.20 ± 0.09	0.13 ± 0.12
L61D <sup>+</sup>	-0.10 ± 0.05	0.39 ± 0.18	-0.13 ± 0.05	0.31 ± 0.11	0.28 ± 0.12
L79D	-0.11 ± 0.05	0.41 ± 0.18	-0.22 ± 0.05	0.53 ± 0.13	0.46 ± 0.18
L98D	-0.25 ± 0.07	0.97 ± 0.27	-0.35 ± 0.08	0.85 ± 0.19	0.78 ± 0.27

TABLE 3: Thermal SZ results from the DR5 f150, DR5 f090, and DR4 ILC map analyses, along with  $1\sigma$  jackknife uncertainty estimates. Dust-corrected stacked tSZ signals  $\delta T_{\text{tSZ}}$  and  $\bar{y}$  are given for the two coadded temperature maps, and  $\bar{y}$  for the DR4 ILC Compton- $y$  map. For the DR5 f150 map, the *Herschel* dust correction is applied, and the uncertainties associated with these corrections are propagated into the cited jackknife uncertainties. For the DR5 f090 map, the *Herschel* dust correction and the f090 beam correction scaling factor are applied. The  $\bar{y}$  results from the disjoint bins shared with C21 (marked as <sup>+</sup>bins) are shown in Figure 8.

# tSZ results

- Average Compton-y in 2.1' aperture from tSZ stacking results
- Measurements consistent across three maps analyzed
- Higher S/N (up to 12 sigma) in higher L bins as expected



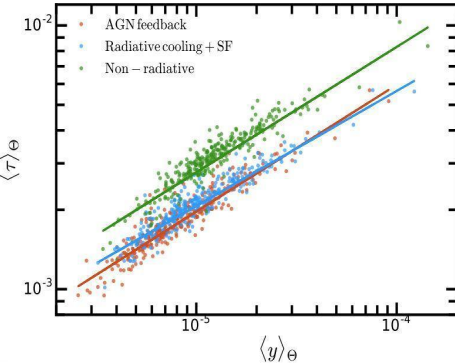
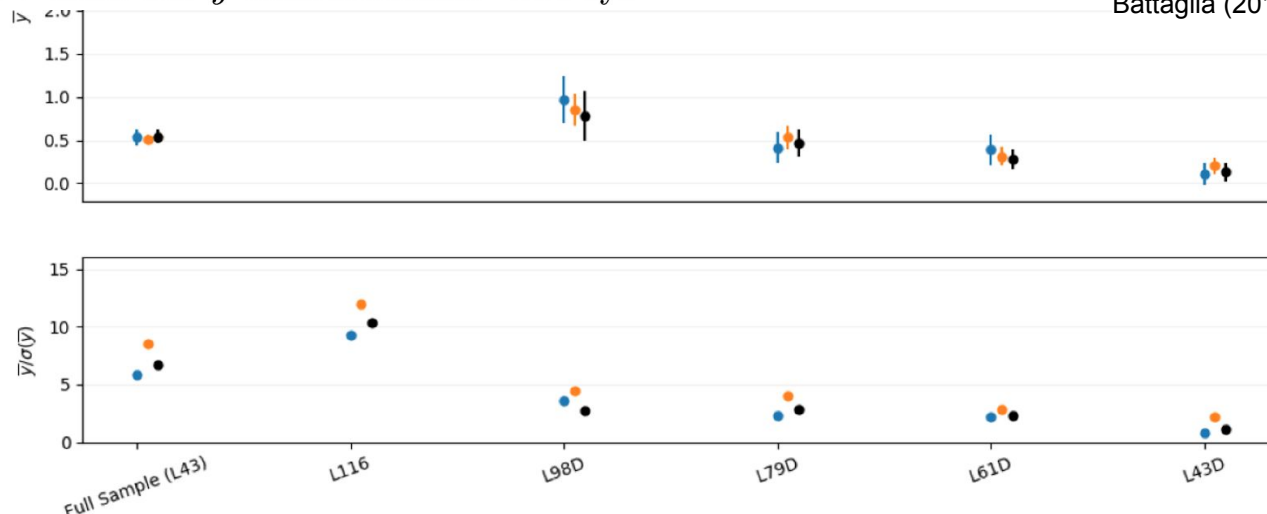
# tSZ results

- From average Compton-y estimate optical depth per bin

In simulations with AGN feedback, Battaglia [3] finds the relationship between  $\bar{y}$  and optical depth to be

$$\ln(\bar{\tau}) = \ln(\tau_0) + m \ln(\bar{y}/10^{-5}) \quad (3)$$

where  $\ln(\tau_0) = -6.40$  and  $m = 0.49$  at  $z = 0.5$ . We use this to estimate  $\bar{\tau}$  from our  $\bar{y}$  measurements. The sys-



Battaglia (2017) 1607.02442

# Optical depth comparisons

- “Theoretical tau” estimated for case in which baryons trace dark matter

For comparison with our measurements, we calculate theoretical estimates for the mean optical depths  $\bar{\tau}_{\text{theory}}$  for each of the luminosity bins. We follow the derivation in Battaglia [3] using an NFW profile to estimate the optical depth in a given aperture,

$$\bar{\tau}_{\text{theory}} = \sigma_T x_e X_H (1 - f_*) f_b \frac{M_{\text{vir}}(< \theta_{2.1'})}{d_A^2 m_p}. \quad (5)$$

Here  $\sigma_T$  is the Thomson cross-section,  $x_e$  is the electron fraction defined as  $x_e = (X_H + 1)/(2X_H)$ ,  $X_H$  is the primordial hydrogen mass fraction ( $X_H = 0.76$ ),  $f_*$  is the stellar mass fraction of the halo,  $f_b$  is the universal baryon fraction ( $\Omega_b/\Omega_M$ ),  $m_p$  is the proton mass, and  $d_A$  is the angular diameter distance to mean redshift of our sample. The parameter value for  $f_b = 0.157$  is set from the cosmological parameters we choose. The value for  $f_*$  is inferred from the stellar mass-halo mass relation from abundance matching as described in [47]. We define the parameter  $f_c = \bar{\tau}_{\text{obs}}/\bar{\tau}_{\text{theory}}$  to compare the estimated  $\bar{\tau}$  values (Table 4) to the theoretically predicted values. This parameter represents the fraction of theoretically predicted optical depth obtained by the two SZ measurements, and is of interest to compare the consistency of the two optical depth estimate methods.

DR5 f150						
Bin	$\bar{\tau}_{\text{theory}}$ $[10^{-4}]$	$\bar{\tau}_{\text{tSZ}}$ $[10^{-4}]$	$\sigma_{\text{sys.}}$ $[10^{-4}]$	$f_{c,\text{tSZ}} \pm (\text{stat., sys.})$	$\bar{\tau}_{\text{kSZ}}$ $[C21]$ $[10^{-4}]$	$f_{c,\text{kSZ}}$
L43**	1.39	1.28 ± 0.10	0.27	0.92 ± (0.07, 0.19)	0.54 ± 0.09	0.39 ± 0.06
L61	1.77	1.55 ± 0.11	0.30	0.88 ± (0.06, 0.17)	0.69 ± 0.11	0.39 ± 0.06
L79 <sup>+</sup>	2.42	1.92 ± 0.10	0.33	0.79 ± (0.04, 0.14)	0.88 ± 0.18	0.36 ± 0.07
L98	3.35	2.55 ± 0.12	0.39	0.76 ± (0.04, 0.12)		
L116	4.44	3.18 ± 0.17	0.43	0.72 ± (0.04, 0.10)		
L43D <sup>+</sup>	0.70	0.59 ± 0.35	0.17	0.85 ± (0.50, 0.24)	0.46 ± 0.24	0.66 ± 0.34
L61D <sup>+</sup>	1.06	1.10 ± 0.25	0.24	1.04 ± (0.24, 0.23)	0.72 ± 0.26	0.68 ± 0.25
L79D	1.53	1.12 ± 0.24	0.25	0.74 ± (0.16, 0.16)		
L98D	2.09	1.71 ± 0.23	0.32	0.82 ± (0.11, 0.15)		
DR5 f090						
Bin	$\bar{\tau}_{\text{theory}}$ $[10^{-4}]$	$\bar{\tau}_{\text{tSZ}}$ $[10^{-4}]$	$\sigma_{\text{sys.}}$ $[10^{-4}]$	$f_{c,\text{tSZ}} \pm (\text{stat., sys.})$	$\bar{\tau}_{\text{kSZ}}$ $[C21]$ $[10^{-4}]$	$f_{c,\text{kSZ}}$
L43**	1.39	1.25 ± 0.07	0.27	0.89 ± (0.05, 0.19)	0.65 ± 0.13	0.47 ± 0.09
L61	1.77	1.46 ± 0.07	0.29	0.82 ± (0.04, 0.16)	0.82 ± 0.17	0.46 ± 0.10
L79 <sup>+</sup>	2.42	1.84 ± 0.08	0.33	0.76 ± (0.03, 0.14)	0.79 ± 0.27	0.33 ± 0.11
L98	3.35	2.35 ± 0.10	0.37	0.70 ± (0.03, 0.11)		
L116	4.44	2.91 ± 0.12	0.41	0.66 ± (0.03, 0.09)		
L43D <sup>+</sup>	0.70	0.79 ± 0.18	0.20	1.14 ± (0.26, 0.29)	0.83 ± 0.34	1.19 ± 0.49
L61D <sup>+</sup>	1.06	0.98 ± 0.18	0.23	0.92 ± (0.17, 0.22)	1.07 ± 0.35	1.01 ± 0.33
L79D	1.53	1.27 ± 0.15	0.27	0.83 ± (0.10, 0.18)		
L98D	2.09	1.60 ± 0.18	0.31	0.77 ± (0.09, 0.15)		
DR4 ILC						
Bin	$\bar{\tau}_{\text{theory}}$ $[10^{-4}]$	$\bar{\tau}_{\text{tSZ}}$ $[10^{-4}]$	$\sigma_{\text{sys.}}$ $[10^{-4}]$	$f_{c,\text{tSZ}} \pm (\text{stat., sys.})$	$\bar{\tau}_{\text{kSZ}}$ $[C21]$ $[10^{-4}]$	$f_{c,\text{kSZ}}$
L43**	1.39	1.29 ± 0.09	0.27	0.92 ± (0.06, 0.19)	0.47 ± 0.12	0.34 ± 0.09
L61	1.77	1.54 ± 0.09	0.30	0.87 ± (0.05, 0.17)	0.74 ± 0.15	0.42 ± 0.08
L79 <sup>+</sup>	2.42	1.96 ± 0.11	0.34	0.81 ± (0.05, 0.14)	0.78 ± 0.23	0.32 ± 0.10
L98	3.35	2.55 ± 0.13	0.39	0.76 ± (0.04, 0.12)		
L116	4.44	3.22 ± 0.15	0.42	0.73 ± (0.03, 0.09)		
L43D <sup>+</sup>	0.70	0.64 ± 0.26	0.17	0.91 ± (0.37, 0.24)	0.18 ± 0.32	0.26 ± 0.46
L61D <sup>+</sup>	1.06	0.93 ± 0.20	0.22	0.88 ± (0.19, 0.21)	0.69 ± 0.34	0.65 ± 0.32
L79D	1.53	1.19 ± 0.20	0.26	0.78 ± (0.13, 0.17)		
L98D	2.09	1.54 ± 0.27	0.30	0.74 ± (0.13, 0.14)		

TABLE 4: Optical depth estimates from the tSZ effect via hydrodynamic simulations,  $1\sigma$  statistical and systematic uncertainties, and fraction of theoretical estimates for mean optical depths ( $f_c$ , Section III.E) for each luminosity bin and analyzed map. Statistical uncertainties on tSZ estimated optical depth are propagated from the tSZ AP jackknife uncertainty estimates and *Herschel* dust corrections. Systematic uncertainties are estimated using the Monte Carlo method taking into account the estimated systematic uncertainties in the  $\bar{\tau}$ - $\bar{\tau}$  relationship from simulations (Equation 3). For example, the  $\bar{\tau}$  fit from the DR5 f150 tSZ results for  $L > 4.30 \times 10^{10} L_\odot$ ,  $1.28 \times 10^{-4}$ , divided by the theoretical  $\bar{\tau}$  estimate of  $1.39 \times 10^{-4}$ , yields  $f_c = 0.92$  for that galaxy sample. Selected  $\bar{\tau}$  estimates from the pairwise kSZ effect from C21 with bootstrap uncertainties are listed along with  $f_c$  for comparison. The fractions for the full galaxy sample (\*\*bin) are shown in Figure 7, and kSZ results from the three disjoint bins shared with C21 (+bins) are shown in Figure 8. Uncertainties on mass estimates from luminosity have not been propagated through to the  $\bar{\tau}_{\text{theory}}$  estimate, so  $f_c$  is best used for comparison and the study of relative trends.

# Systematics discussion

---

- Herschel dust corrections partially address source galaxy emission, residual dust contamination can be seen but is  $< 1$  sigma
- Galactic plane mask for synchrotron emission
- Future work could improve upon our results by modeling and removing dust and synchrotron emission from the LRGs
- Two-halo term estimated and found to be  $< 1$  sigma, but will be important to correct for in future higher S/N work
- Mass considerations: simulation relationship and uncertainty propagation